NONLINEAR MODELLING OF AN IMMERSED TRANSMITTING CAPACITIVE MICROMACHINED ULTRASONIC TRANSDUCER FOR HARMONIC BALANCE ANALYSIS

A THESIS

SUBMITTED TO THE DEPARTMENT OF ELECTRICAL AND

ELECTRONICS ENGINEERING

AND THE INSTITUTE OF ENGINEERING AND SCIENCES

OF BILKENT UNIVERSITY

IN PARTIAL FULFILLMENT OF THE REQUIREMENTS

FOR THE DEGREE OF

MASTER OF SCIENCE

By

Hüseyin Kağan Oğuz

July 2009

I certify that I have read this thesis and that in my opinion it is fully adequate, in scope and in quality, as a thesis for the degree of Master of Science.

Prof. Dr. Hayrettin Köymen(Supervisor)

I certify that I have read this thesis and that in my opinion it is fully adequate, in scope and in quality, as a thesis for the degree of Master of Science.

Prof. Dr. Abdullah Atalar

I certify that I have read this thesis and that in my opinion it is fully adequate, in scope and in quality, as a thesis for the degree of Master of Science.

Assist. Prof. Dr. Arif Sanlı Ergün

Approved for the Institute of Engineering and Sciences:

Prof. Dr. Mehmet Baray
Director of Institute of Engineering and Sciences

ABSTRACT

NONLINEAR MODELLING OF AN IMMERSED TRANSMITTING CAPACITIVE MICROMACHINED ULTRASONIC TRANSDUCER FOR HARMONIC BALANCE ANALYSIS

Hüseyin Kağan Oğuz
M.S. in Electrical and Electronics Engineering
Supervisor: Prof. Dr. Hayrettin Köymen
July 2009

Finite element method (FEM) is used for transient dynamic analysis of capacitive micromachined ultrasonic transducers (CMUT), which is particularly useful when the membranes are driven in the nonlinear regime. A transient FEM analysis shows that CMUT exhibits strong nonlinear behavior even at very low AC excitation under DC bias. One major disadvantage of FEM is the excessive time required for simulation. Harmonic Balance (HB) analysis, on the other hand, provides an accurate estimate of the steady-state response of nonlinear circuits very quickly. It is common to use Mason's equivalent circuit to model the mechanical section of CMUT. However, it is not appropriate to terminate Mason's mechanical LC section by a rigid piston's radiation impedance, especially, for an immersed CMUT. We studied the membrane behavior using a transient FEM analysis and found out that for a wide range of harmonics around the series resonance, the membrane displacement can be modeled as a clamped radiator. We considered the root mean square of the velocity distribution on the membrane surface as the circuit variable rather than the average velocity. With this

definition the kinetic energy of the membrane mass is the same as that in the model. We derived the force and current equations for a clamped radiator and implemented them in a commercial HB simulator. We observed much better agreement between FEM and the proposed equivalent model, compared to the conventional model.

Keywords: CMUT, nonlinear modeling, equivalent circuit, harmonic balance, transient analysis.

ÖZET

SUYLA YÜKLENMİŞ KAPASİTİF MİKROİŞLENMİŞ ULTRASONİK ÇEVİRİCİLERİN HARMONİK DENGE ANALİZİ İÇİN DOĞRUSAL OLMAYAN MODELİ

Hüseyin Kağan Oğuz
Elektrik ve Elektronik Mühendisliği Bölümü Yüksek Lisans
Tez Yöneticisi: Prof. Dr. Hayrettin Köymen
Temmuz 2009

Sonlu eleman methodu (SEM) kapasitif mikroişlenmiş ultrasonik çeviricilerin (KMUÇ) geçici dinamik rejim analizinde kullanılmakta ve özellikle de membranlar doğrusal olmayan şekilde sürüldüğünde faydalıdır. Geçici rejim SEM analizi, DC gerilim altında çok düşük AC uyarımda dahi KMUÇ'un şiddetli bir şekilde doğrusal olmayan davranış sergilediğini göstermektedir. SEM'in başlıca dezavantajlarından bir tanesi, simulasyon için aşırı zaman gerektirmesidir. Diğer taraftan, Harmonik Denge (HD) analizi, doğrusal olmayan devrelerin denge durumundaki tepkisinin doğru tahminini çok hızlı sağlamaktadır. KMUÇ'un mekanik kısmını modellemek için Mason'ın eşdeğer devresi yaygın olarak kullanılmaktadır. Fakat, özellikle, daldırılmış bir KMUÇ için Mason'ın mekanik LC kısmını katı bir pistonun radyasyon empedansı ile sonlandırmak uygun değildir. Geçici rejim SEM analizini kullanarak membran davranışını araştırdık ve membran hareketinin seri rezonans civarındaki birçok harmoniklerinin yanlarından tutturulmuş bir ışıyıcı olarak modellenebildiğini bulduk. Devre elemanı olarak ortalama hız yerine, membran yüzeyindeki hız dağılımının etkin değerini dikkate aldık. Bu tanım ile membran ağırlığının kinetik enejisi modeldeki ile aynıdır. Yanlarından

tutturulmuş bir ışıyıcı için kuvvet ve akım denklemlerini türettik ve ticari bir HD simülatörü kullanarak bunları modelde uyguladık. Olağan modele göre, SEM ile önerilen eşdeğer model arasında çok daha iyi uyuşma gözlemledik.

Anahtar Kelimeler: KMUÇ, doğrusal olmayan modelleme, eşdeğer devre, harmonik denge, geçici rejim analizi.

ACKNOWLEDGMENTS

I would like to express my sincere gratitude to my supervisor Prof. Dr. Hayrettin Köymen for his invaluable guidance and instructive comments through the development of this thesis. His encouragements enabled the completion of this work.

I am grateful to Prof. Dr. Abdullah Atalar for his valuable feedback and contributions. I would also like to express my special thanks to him and to Assist. Prof. Dr. Arif Sanlı Ergün for evaluating my thesis as the jury members.

Thanks to my friends Selim, Niyazi, Vahdettin, Burak and Hakan for their discussions and suggestions at every time I needed.

I would also like to thank TUBITAK for funding my studies through the project grant 107T921.

Lastly, many thanks to my beloved family and my fiance Tuğba for their endless love and support.

Contents

List of Figures

List of Tables

Chapter 1

INTRODUCTION

Capacitive micromachined ultrasonic transducer (CMUT) is a metalized membrane suspended above a silicon substrate with a small spacing, in submicrometer range, to form a capacitor. The membrane material is generally silicon nitride, where the top electrode is located either at the top or bottom of the membrane. When a voltage is applied between the membrane electrode and the bottom electrode located on the substrate, the membrane is attracted by electrostatic forces and the induced stress within the membrane balances the attraction. A CMUT can operate both as a receiver and a transmitter, such that, driving the membrane by an alternating voltage generates ultrasound and conversely, when a DC biased membrane is exposed to ultrasound, current is produced due to capacitance variation under constant bias. A single CMUT cell is shown in Fig. 1.1.

CMUTs are widely designed and fabricated in the past decade [1]. CMUTs with some unique capabilities attracted attention of applications such as medical imaging, high intensity focused ultrasound, intravascular ultrasound, airborne acoustics, microphones and nondestructive evaluation. Fabrication of CMUTs for those applications requires tedious process steps which is time consuming and

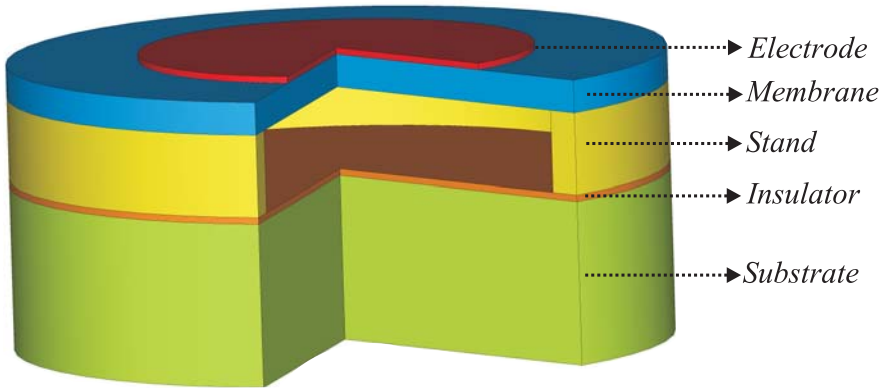

Figure 1.1: 3D view of a CMUT cell.

expensive [2,3]. Therefore, an accurate and fast simulation method is needed for designing CMUTs.

The efforts for simulating the CMUTs have started with the development of an equivalent circuit model [1], based on Mason's equivalent circuit [4] for electro-acoustic devices. Different models for defining the equivalent circuit elements are available in the literature [1,5–7]. However, finite element method simulations are still needed [8] in order to simulate the CMUT operation including the nonlinear effects, medium loading, cross talk and the effect of the higher order harmonics. Recently, fully analytical models are developed for fast and efficient results of frequency response analysis [9]. FEM simulation packages—such as ANSYS—are powerful tools and extensively used for the analysis of CMUTs. FEM analysis predicts the performance of a particular design very well and hence it is a very good testing and tuning tool. However, the computational expense required for the solution makes FEM tools unsuitable for using them in design stage. For instance, transient dynamic analysis of a CMUT is crucial in order to understand the nonlinear behavior of the CMUT, however, it has high computational cost and requires many cycles to reach the steady state. It does not rapidly respond when a parameter is altered and hence, an idea about its effect cannot be instantly grasped by the designer. Calculated design charts for large array of circular

CMUTs are available in the literature [10] but lacks the nonlinear effects when the CMUTs are driven with a high excitation voltage. In recent years, the efforts for modelling the nonlinear behavior of CMUTs under large excitations [6, 11] have increased due to the emerging need for the applications that require nonlinear excitation [12–16].

In this work, we have developed an equivalent circuit, which takes into account the non-uniform velocity distribution across a membrane and predicts the nonlinear behavior of a circular CMUT membrane. This model is based only on the physics of the device and does not employ FEM for any parameter determination. The equivalent circuit accurately includes the effect of the immersion medium loading. A linear equivalent circuit model can predict the small signal behavior of CMUT, however, CMUT exhibits strong nonlinear behavior even at very low AC excitation. A linear mechanical section in the equivalent circuit with a consistent radiation impedance is solved by harmonic balance (HB) analysis. We perform transient and harmonic balance simulations and show that the results are consistent with the FEM results.

In diagnostic imaging, the discovery of harmonic imaging offered many improvements, such as better spatial and contrast resolution, over the regular fundamental imaging. Harmonic imaging is an advanced technique, which forms the ultrasound image from the backscattered signal at twice the frequency of transmitted signal. However, the limited transducer bandwidth decreases the bandwidth of both receive and transmit signals [17]. Often, separate transducers are employed for transmission and reception. CMUT arrays have large bandwidth, which can accommodate both of these signals in the same transducer. However, excitation signal must be pre-distorted in order to avoid the distortion at the acoustic radiation. We have demonstrated the use of the proposed equivalent circuit model, by designing the time-waveform of the excitation signal to obtain the given acoustic radiation signal at the output of the CMUT. Utilizing

the equivalent model equations and parameters in MATLAB, we calculate the required electrical excitation.

Chapter 2 gives an introduction about finite element and equivalent circuit modeling of CMUTs. Mason's equivalent circuit parameters are briefly explained. Chapter 3 presents an equivalent circuit model, where the root mean square velocity distribution on the membrane surface is employed as the circuit variable rather than the average velocity in Mason's model. Clamped membrane velocity profile is taken into consideration together with the consistent radiation impedance. In chapter 4, the physical equations of the CMUT are derived using the analytical expression that Greenspan [18] studied for clamped radiator velocity profile. Chapter 5 represents the use of the developed equivalent circuit for linear and nonlinear analysis of transmitting CMUTs, where the predictions of the model are compared with static, transient and harmonic FEM analyses results. The last chapter concludes the work done.

Chapter 2

Modelling of CMUTs

There are mainly two types of modeling techniques for CMUTs: mathematical or equivalent circuit modeling and FEM simulation based modeling. For the first one, the analogy between the electrical circuits and the mechanical systems is widely utilized in order to construct the electrical equivalent circuit of electromechanical systems [4], which comprise both of these domains.

Physical phenomenon in many engineering applications might be explained in terms of partial differential equations, which can be solved analytically unless the shapes considered are not very complex. The equivalent circuit modeling of CMUTs begin by solving the differential equation of the membrane motion and then, calculating the mechanical impedance of the membrane [4]. On the other hand, the idea of dividing a particular shape into *finite elements* connected by *nodes* in Finite Element Method (FEM), makes it is possible to analyze amorphous bodies. As a matter of fact, finite element solution converges to the precise partial differential solution as the number of finite elements increase. FEM provides very accurate solutions for several problems including structural, thermal, electromagnetic, fluids, multi-body and coupled-field environments by using a numerical approach.

In this thesis, we study the modeling of immersed transmitting CMUTs, in order to facilitate the design of systems established by transducers that exhibit nonlinear behavior. Transient, steady-state and frequency response of CMUT cells are analyzed rapidly and intuitively, where FEM results are also employed for comparison with the prediction of the equivalent circuit.

2.1 Finite Element Modeling

We use ANSYS[1], a commercially available FEM software package, which is a comprehensive tool capable of solving different coupled physical phenomena in a single simulation environment. Among several types of analyses, transient dynamic analysis is particularly useful when the CMUTs are driven in the nonlinear regime, where large deflections in the finite element model can also be taken into account to obtain more accurate results.

Modeling is the major step where you can construct, optimize and check the specifications of an entire design before the fabrication. FEM has significantly improved the methodology of the design process in many engineering applications and achieved the desired level of accuracy required. We constructed a finite element model in ANSYS, where acoustic problems such as pressure distribution and particle velocity can be solved. A coupled acoustic analysis in ANSYS takes into account the interaction between the fluid medium and surrounding structure. Transient dynamic analysis of an immersed CMUT cell is implemented in a compressible but non-flowing fluid medium to solve the electrostatic and harmonic generation problems. It is possible to determine the dynamic response of a structure under time-dependent loads, however, transient analysis lasts after a long time, since it takes many cycles to reach steady state.

[1]ANSYS,Inc, www.ansys.com

2-D axisymmetric plane elements are used to build the FEM model shown in Fig. 2.1, such that a CMUT membrane is replicated around the lateral plane. Similar models are also built [8], since the model is adequate and preferable in order to reduce the computational time required for the simulations. PLANE42 element type is used to model the membrane, which is suitable for solid structures. The element has stress stiffening and large deflection features. We specify membrane's density, Young's modulus and Poisson's ratio.

The electrical ports exist in the electro-mechanical transducer elements, TRANS126, which convert energy from a structural domain into electrostatic domain and vice versa. Fluid medium is formed by 2-D FLUID29 elements, which couple the acoustic pressure and structural displacement at the fluid-solid interface. The circular periphery of the fluid medium is surrounded by absorbing boundary elements, which simulate the outgoing effects of pressure waves that extend to infinity.

2.2 Electrical Equivalent Circuit

Studies about the theory of bending structures evolved into equivalent circuit models in order to facilitate the design of transducers. Analyses of capacitive ultrasonic transducers are discussed for many decades [1]. Mason derived the expression of the mechanical impedance of an unbiased thin membrane and used it in an electrical model [4]. Mason's small signal equivalent circuit is shown in Fig. 2.2, where Z_m is the lumped mechanical impedance, C_0 is the shunt input capacitance, n is the transformer ratio, Z_a is the mechanical impedance of the immersion medium and S is the area of the membrane.

Mason's circuit is a two port network which is composed of electrical and mechanical domains, which represents voltage-current and force-velocity pairs, respectively. This equivalent circuit is designed to operate both as a receiver

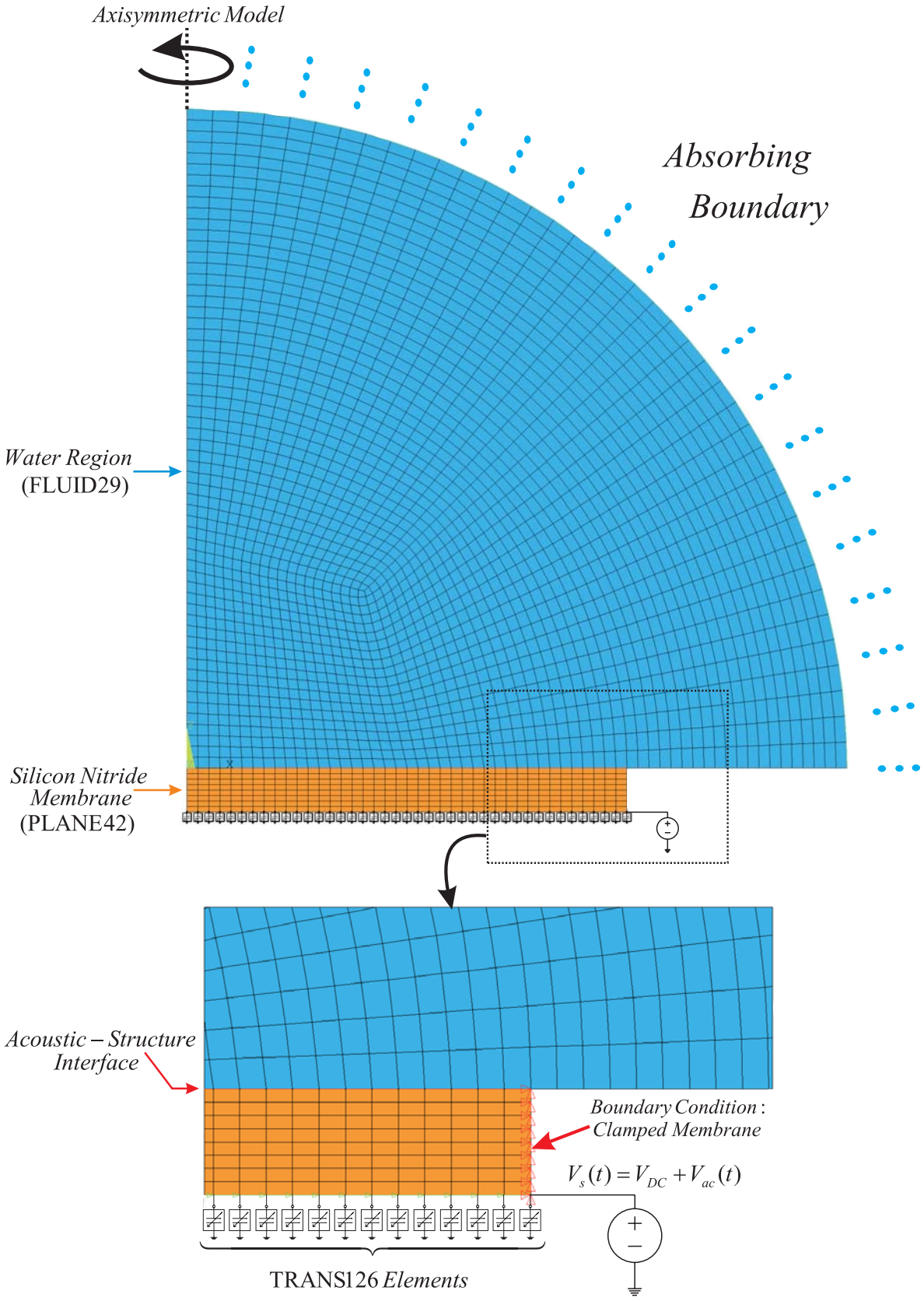

Figure 2.1: Finite Element Model of the CMUT.

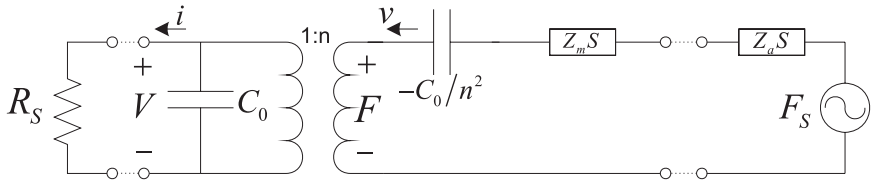

(a)

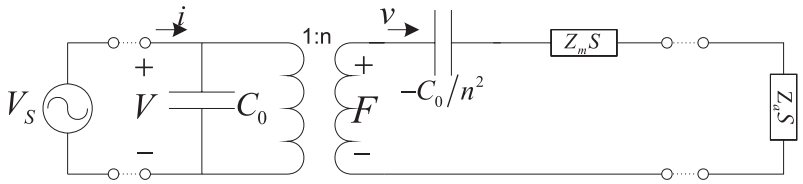

(b)

Figure 2.2: Mason's small signal equivalent model (a) for a CMUT configured as a receiver, where the incident acoustic signal (F_s) is monitored by the current flowing through the load resistance of the receiver (R_s), (b) for a CMUT configured as a transmitter driving the medium impedance ($Z_a S$).

and an emitter under certain assumptions. Firstly, CMUT must not be operated near the collapse point, which is an important drawback, because in receive mode CMUTs are usually intended to function near the collapse point to be more sensitive to incoming acoustic waves and to obtain better electromechanical energy conversion. Secondly, the model is only valid under small signal conditions when the applied bias voltage does not cause a significant spring softening. Electrical circuit parameters emerged from the theory with these assumptions are briefly discussed below.

Mason derived the mechanical impedance of an unbiased circular membrane, which has a radius of a, Young's modulus Y_0 and Poisson's ratio σ, from the variation equation of motion [4]. He found the potential energy difference of a thin membrane that experiences a surface normal displacement of $x(r)$. The major assumption with this energy formulation is that any tension created due to

normal displacement $x(r)$ is insignificant compared to the initial tension within the membrane.

- **Mechanical Impedance**, Z_m is the mechanical impedance of the membrane in vacuum. A uniform pressure distribution, P, is assumed on the membrane with surface area S, which implies a total force of PS. The velocity of the membrane is $v(r) = jwx(r)$, where r, is the radial position on the membrane and the lumped average velocity $\bar{v}$ is defined as

$$\bar{v} = \frac{1}{\pi a^2} \int_0^a \int_0^{2\pi} v(r) r d\theta dr \tag{2.1}$$

  Then mechanical impedance is the ratio of pressure to velocity, $Z_m = P/\bar{v}$. It is feasible to obtain Z_m as lumped elements in order to model the unequally spaced mechanical resonances. Fig. 2.3 shows the normalized mechanical impedance of the CMUT with respect to material properties and device dimensions. This impedance expression might be replaced with a series LC section to predict the operations at frequencies around the series resonance frequency [1, 5]. It is sufficient to match the model impedance found by FEM with the Mason's expression [5] at the first series resonance frequency.

- **Turns Ratio**, n, transforms velocity at the mechanical domain, into electrical current. In order to operate, CMUTs are first deflected by a DC bias, on which a sinusoidal voltage is superimposed. Let the total voltage between the electrodes be $V = V_{DC} + V_{ac}\sin(wt)$, where $V_{ac} \ll V_{DC}$ is the small signal AC voltage. Then, the current flowing through the transducer is

$$I = \frac{dQ(t)}{dt} = \frac{d}{dt}(C(t)V(t)) = C(t)\frac{dV(t)}{dt} + V(t)\frac{dC(t)}{dt} \tag{2.2}$$

  where $C(t)$ is the electrical input capacitance of a CMUT with gap height t_g and insulator thickness t_i :

$$C(t) = \frac{\epsilon_0 \epsilon S}{\epsilon_0 t_i + \epsilon t_g(t)} \tag{2.3}$$

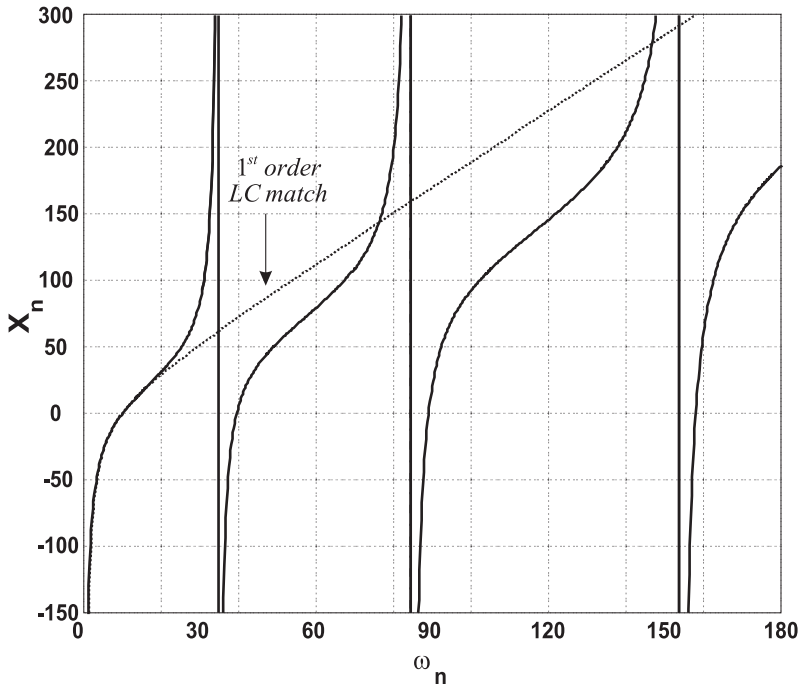

Figure 2.3: Comparison of the agreement between the mechanical impedance and the Mason's impedance expression around the first series resonance frequency.

Since, this is a small signal analysis, capacitance can be expressed by $C(t) = C_0 + C_{ac}\sin(wt + \phi)$ where $C_{ac} \ll C_0$. Hence, Eq. (2.2) can be rewritten as

$$I \approx C_0 \frac{dV_{ac}(t)}{dt} + V_{DC} \frac{dC_{ac}(t)}{dt} \tag{2.4}$$

which is further expanded by taking the derivative of C_{ac} :

$$I \approx C_0 \frac{dV_{ac}(t)}{dt} - V_{DC} \frac{\epsilon_0 \epsilon S}{(\epsilon_0 t_i + \epsilon t_{g_0})^2} \frac{dt_g(t)}{dt} \tag{2.5}$$

The derivative of the gap height, t_g, is equal to the average velocity, $\bar{v}$. Therefore, the term in front of it appears to be the turns ratio, n, since, it transforms velocity into electrical current.

$$n = \frac{V_{DC}\epsilon_0 \epsilon^2 S}{(\epsilon_0 t_i + \epsilon t_{g_0})^2} \tag{2.6}$$

It is apparent that this small signal transformer ratio is dependent on the bias voltage, the DC value of the gap height, t_{g_0}, the insulator layer thickness,t_i, and the dielectric constant ϵ.

- **Spring Softening Capacitance**, $-C_0/n^2$, is included in series with the mechanical impedance Z_m. When the top electrode undergoes a displacement towards the bottom electrode while a force is acting on it, stress within the membrane opposes the attraction. In addition, as the electrodes draw near to each other under constant V_{DC}, electrostatic force increases. This event is known as spring softening effect.

Chapter 3

Root Mean Square (RMS) Equivalent Circuit

It is common to use Mason's equivalent circuit to model the mechanical section of a CMUT [1, 4]. Mason's circuit is comprised of a series LC section, where L represents the equivalent mass and C stands for the inverse of the spring constant of the membrane. In this equivalent circuit, the through and across variables are the average particle velocity and the total force, respectively. In vacuum, where the medium loading is zero, Mason's mechanical section accurately models the results obtained by FEM simulation [5]. In this model the equivalent mass (L) becomes 1.8 times the mass of the membrane as stated by Mason [4].

When the device is immersed, it is necessary to consider the terminating radiation impedance in the equivalent circuit in order to represent the device behavior correctly. The radiation impedance of an aperture is determined by the particle velocity distribution across the aperture. It is the ratio of total power radiated from the transducer to the square of the absolute value of a nonzero reference velocity. Therefore, the through and across lumped variables must be

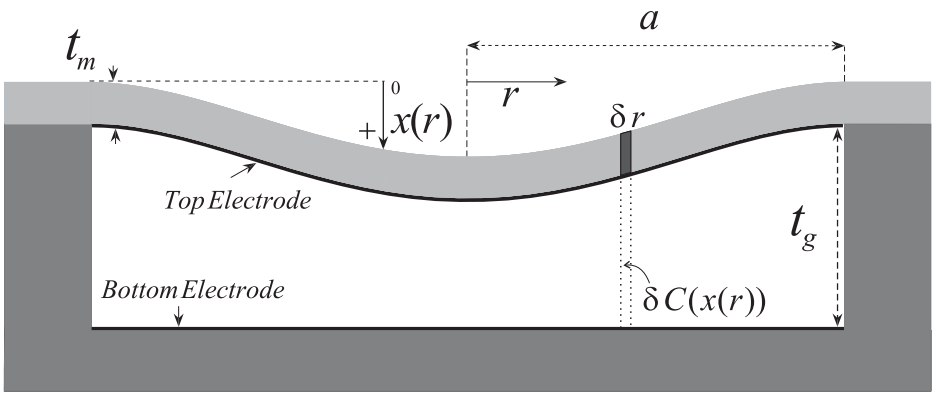

Figure 3.1: CMUT Geometry.

defined in such a way that they are consistent both in the equivalent circuit model and in the radiation impedance.

3.1 Velocity Profile and the Radiation Impedance

The acoustic radiation from radiators with nonuniform velocity profiles are studied by Greenspan [18]. The particle displacement and the velocity profile across circular clamped membranes are not uniform and can be very well approximated by the profiles that Greenspan studied:

$$v(r) = (n+1)v_{avg}\left[1 - \frac{r^2}{a^2}\right]^n \quad \text{for } r < a \tag{3.1}$$

where a is the radius of the aperture, r is the radial position, v_{avg} is the average velocity along the membrane surface and n is a constant that specifies the type of the profile. If $n = 0$, then (3.1) stands for the profile of a rigid piston. For a clamped membrane, as the CMUT shown in Fig. 3.1, $n = 2$ approximates the nonuniform profile. The radiation impedance of a velocity profile similar to that of a CMUT is given as "normalized radiated power" of a "clamped radiator" ($n = 2$) in [18].

When the CMUT is immersed in water, it is reasonable to assume that the electro-mechanical behavior, hence the model, of the membrane remains intact.

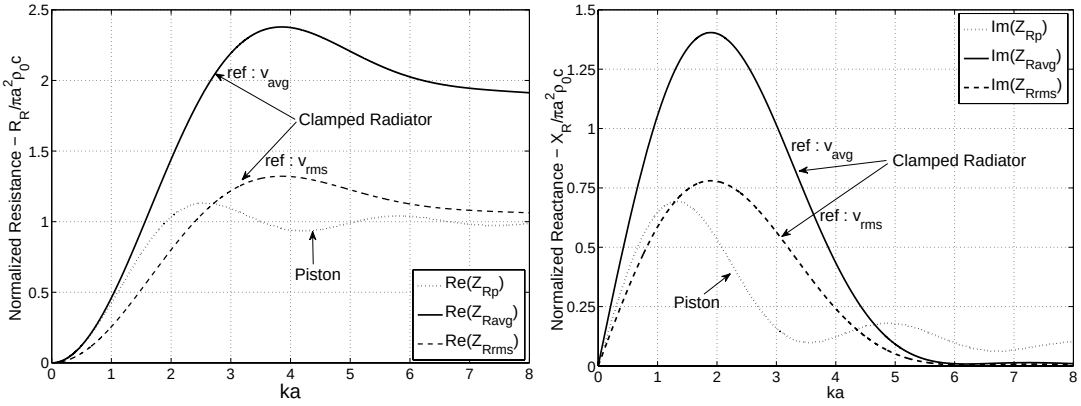

(a) (b)

Figure 3.2: (a) Real (resistive) and (b) imaginary (reactive) parts of the radiation impedance of the piston and the clamped radiator normalized to $\pi a^2 \rho_0 c$, where ρ_0 and c are the density and the velocity of sound in the immersion medium. For clamped radiator both average and rms velocity of the membrane are used as the reference velocity and shown separately.

However, interaction between the membrane and the medium loads the mechanical section. In Fig. 3.2, the real and imaginary parts of the normalized radiation impedance of the piston radiator, Z_{Rp}, and the clamped radiator, Z_{Ravg}, are shown with respect to ka, where k is the wave number. Mason's circuit and the radiation impedance Z_{Ravg} are compatible, since the through lumped variable in both is the average velocity, v_{avg}. Z_{Ravg} is considerably different than Z_{Rp} of a piston as depicted in Fig. 3.2. For example, the real part of Z_{Ravg} is 1.8 times that of Z_{Rp} for large ka.

Inadequacy of terminating Mason's mechanical LC section by a rigid piston's radiation impedance in water, to model the immersed CMUT, is demonstrated in [19, 20]. This is due to the fact that, a rigid piston has a uniform velocity profile ($n = 0$), whereas CMUT can be better approximated by $n = 2$ in (3.1). The real part (resistive) of Z_{Rp} and Z_{Ravg} are similar for $ka < 1$ as depicted in Fig. 3.2(a), whereas the reactive parts are not. Considering this difference and the fact that Mason's mechanical impedance is derived based on the clamped membrane boundary conditions, it is not appropriate to combine Mason's model with the piston radiation impedance.

3.2 Root Mean Square (rms) Velocity

The average velocity is not an appropriate lumped variable to determine the kinetic energy of the membrane, which is a distributed system. The kinetic energy calculated using the mass of the membrane and average velocity is less than the actual energy of the membrane. The kinetic energy, E_K, of the membrane mass is

$$\begin{aligned} E_K &= \int_0^{2\pi}\int_0^a \frac{1}{2} v(r) v^*(r) \rho t_m r \, \mathrm{d}r \, \mathrm{d}\theta \\ &= \frac{1}{2}(\rho t_m \pi a^2) \left[\frac{1}{\pi a^2} \int_0^{2\pi}\int_0^a v(r) v^*(r) r \, \mathrm{d}r \, \mathrm{d}\theta \right] \end{aligned} \tag{3.2}$$

where $v(r)$ is the velocity normal to the surface of the membrane, ρ is the density, t_m is the thickness and $\rho t_m \pi a^2$ is the total mass of the membrane. The term in square brackets is the square of rms velocity:

$$v_{rms} = \sqrt{\frac{1}{\pi a^2} \int_0^{2\pi}\int_0^a v(r) v^*(r) r \, \mathrm{d}r \, \mathrm{d}\theta} \tag{3.3}$$

Hence an equivalent circuit model can preserve the kinetic energy in (3.2) only if rms velocity is employed as the through variable. For a rigid piston ($n = 0$), both average and rms velocity are equal and the model parameters are the same. The relationship between the average velocity, v_{avg}, the rms velocity, v_{rms} and the peak velocity at the center of the membrane, v_p, are

$$v_{rms} = \frac{n+1}{\sqrt{2n+1}} v_{avg} \quad \text{and} \quad v_p = (n+1) v_{avg} \tag{3.4}$$

For $n = 2$, $|v_{rms}|^2 = 1.8 |v_{avg}|^2$.

3.3 RMS Equivalent Circuit Model Parameters

In order to derive an equivalent circuit with the rms velocity as the through variable, we consider the mechanical impedance of a clamped membrane in vacuum.

We begin by defining the mechanical impedance as the ratio of total power across the driven surface of the membrane and the square of v_{rms},

$$Z_{rms} = \frac{Pw_{Total}}{|v_{rms}|^2} = \frac{\int_0^a 2\pi p(r) v^*(r) r \, \mathrm{d}r}{|v_{rms}|^2} \tag{3.5}$$

where $p(r)$ is the normal force per unit area distribution on the driven surface. Assuming that $p(r)$ is constant across the membrane surface and $n = 2$ for clamped membrane, this impedance expression becomes $|v_{avg}|^2/|v_{rms}|^2$ times the Mason's equivalent circuit mechanical impedance obtained from the total force to average velocity ratio. Z_{rms} can readily be calculated by FEM analysis. Matching the slope of the impedance of an equivalent series LC section to (3.5) at the resonance frequency reveals that L_{rms} is exactly equal to the mass of the membrane, rather than 1.8 times the mass as in Mason's circuit.

$$L_{rms} = \rho t_m \pi a^2 \tag{3.6}$$

Hence, the lumped inductance in the rms circuit models the effect of mass directly. In order to preserve the resonance frequency in vacuum, the capacitance in Mason's circuit representing the compliance of the membrane must be multiplied with $|v_{rms}|^2/|v_{avg}|^2 = 1.8$

$$C_{rms} = 1.8 \frac{(1-\sigma^2)\, a^2}{16\pi Y_0 t_m^3} \tag{3.7}$$

where Y_0 is the Young's modulus and σ is the Poisson's ratio of the membrane material and t_m is the membrane thickness. A correction to this formula may be necessary for membranes with $t_m/a > 0.1$ as explained in [5]:

$$C_{rms} = \frac{|v_{rms}|^2}{|v_{av}|^2} \frac{12a^2\,(1-\sigma^2)}{\pi Y_0 t_m^3} \left[q_3 \left(\frac{t_m}{a}\right)^3 + q_2 \left(\frac{t_m}{a}\right)^2 + q_1 \left(\frac{t_m}{a}\right) + q_0 \right] \tag{3.8}$$

where the polynomial coefficients q_i for a first order LC model are given in Table 3.3.

If v_{rms} is employed in the "normalized power" expression instead of v_{avg}, we obtain the normalized radiation impedance Z_{Rrms}, depicted in Fig. 3.2, which is

q_3	q_2	q_1	q_0
-0.007167	0.03620	-0.0005467	0.005208

Table 3.1: Coefficients of Eq. 3.8.

$|v_{avg}|^2/|v_{rms}|^2$ times the "normalized power" in [18]. Calculation of Z_{Rrms} can be found in the Appendix.

Mechanical section of the rms equivalent circuit is depicted in Fig.3.3, where F_{tot} is the total force on the membrane surface.

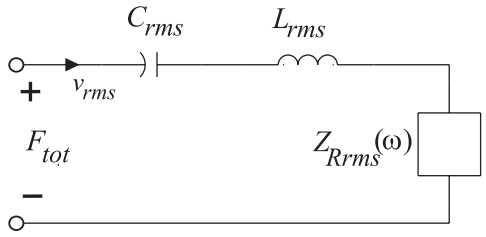

Figure 3.3: Mechanical section of the rms circuit.

Chapter 4

Fundamental Equations of the CMUT

Static and harmonic analyses in FEM can only provide the DC deflection and the fundamental velocity profile, respectively. We studied the membrane behavior using dynamic transient FEM analysis and at 80 discrete radial positions along the membrane surface, we fitted a sum of sinusoids, which consists of the fundamental and its first five harmonics, to each of the time-domain velocity data obtained at these 80 locations along the radius. Then, the amplitude distribution of each harmonic along the radius is used to find the velocity profile at that frequency. The phase of each harmonic is observed to be almost constant across the radius. We fitted (3.1) to the obtained velocity profile of each harmonic component and we observed that n in (3.1) is dependent on the bias voltage and varies between 1.95 and 2.25. This is demonstrated in Fig. 4.1, where the first three harmonics of the velocity profile is depicted. In Fig. 4.1(a), 50V DC bias and 20V peak AC signal is applied at half the resonance frequency. In Fig. 4.1(b), 85V DC bias and 5V peak AC signal is applied at one fourth of the resonance frequency. As the bias voltage increases, n also increases. Nevertheless, the membrane velocity

profile can be modelled quite accurately as a clamped radiator ($n = 2$), up to more than two times the series resonance frequency.

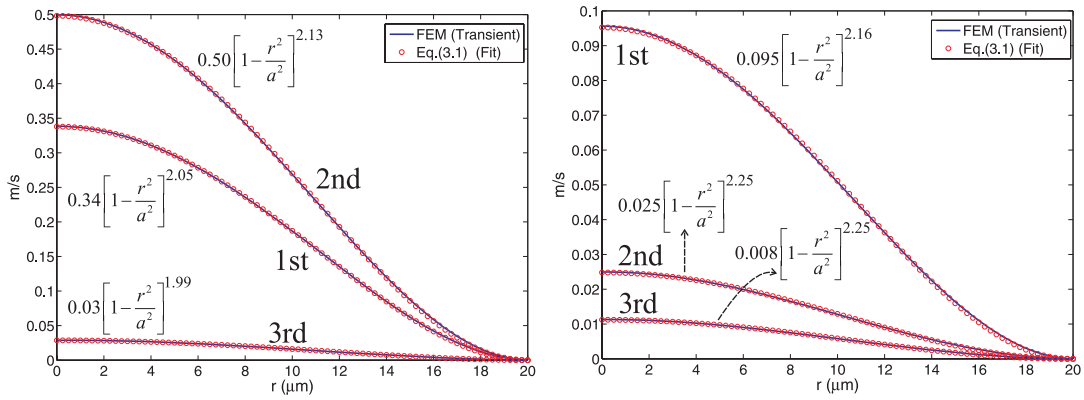

(a) (b)

Figure 4.1: The velocity profile of the first three harmonics found by FEM transient analysis and the results obtained by fitting (3.1) to each of them. (a) 50V DC bias and 20V peak AC signal is applied at 2.5MHz. (b) 85V DC bias and 5V peak AC signal is applied at 1MHz.

It is possible to derive a nonlinear analytical electro-mechanical model for the CMUT. When the CMUT is driven by a voltage $V(t) = V_{DC} + V_{ac}(t)$, the electrostatic force acting on the small ring of area $2\pi r\,\delta r$ can be calculated by taking the derivative of the stored energy in the clamped capacitance

$$\delta F(r,t) = \frac{1}{2}V^2(t)\frac{\mathrm{d}\left[\delta C(x(r,t))\right]}{\mathrm{d}x} \tag{4.1}$$

where $x(r,t)$ is the membrane displacement normal to the surface and the capacitance of the ring is

$$\delta C(x(r,t)) = \frac{\epsilon_0 2\pi r\,\delta r}{t_g - x(r,t)} \tag{4.2}$$

Total force on the driven surface of the membrane is found by integrating (4.1) as $\delta r \to 0$

$$F_{tot}(t) = \epsilon_0 \pi V^2(t) \int_0^a \frac{r\,\mathrm{d}r}{\left[t_g - x_p(t)(1 - r^2/a^2)^n\right]^2} \tag{4.3}$$

where t_g is the gap height, ϵ_0 is the free space permittivity and $x_p(t) = x(0,t)$ is the peak displacement at the center of the membrane. Equation (4.3) can be

evaluated for $n = 2$ as follows

$$F_{tot}(t) = \frac{C_0 V^2(t)}{4t_g}\left[\frac{t_g}{t_g - x_p(t)} + \frac{\tanh^{-1}\left(\sqrt{\frac{\mathrm{x_p(t)}}{\mathrm{t_g}}}\right)}{\sqrt{\frac{x_p(t)}{t_g}}}\right] \tag{4.4}$$

where $C_0 = \epsilon_0 \pi a^2/t_g$. Note that when $x_p(t) < 0$

$$\frac{\tanh^{-1}\left(\sqrt{x_p(t)/t_g}\right)}{\sqrt{x_p(t)/t_g}} = \frac{\tan^{-1}\left(\sqrt{-\mathrm{x_p(t)/t_g}}\right)}{\sqrt{-x_p(t)/t_g}} \tag{4.5}$$

which is a more useful expression for a simulator.

For small displacements around the point $x_p(t) = 0$, Taylor series expansion of (4.4) provides a simpler mathematical interpretation, where the leading terms are

$$F_{tot}(t) \approx \frac{C_0 V^2(t)}{2t_g}\left[1 + \frac{2}{3}\frac{x_p(t)}{t_g} + \frac{3}{5}\left(\frac{x_p(t)}{t_g}\right)^2\right] \tag{4.6}$$

The current flowing through the electrodes of the small ring is the time derivative of the charge on this ring

$$\frac{\mathrm{d}\left[\delta Q(r,t)\right]}{\mathrm{d}t} = \delta C(x(r,t))\frac{\mathrm{d}V(t)}{\mathrm{d}t} + \frac{\mathrm{d}\left[\delta C(x(r,t))\right]}{\mathrm{d}t}V(t) \tag{4.7}$$

The first term in (4.7) is the capacitive current and the second one is induced by the membrane motion and therefore, we call it the velocity current. We note that both current components depend on the instantaneous value of the membrane displacement. Considering an equivalent circuit, capacitive current flows through the shunt capacitance at the electrical side and velocity current is the one that gives rise to velocity at the mechanical port. To find the total capacitive current, i_{cap}, we evaluate the integral as $\delta r \to 0$

$$\begin{aligned} i_{cap}(t) &= \frac{\mathrm{d}V(t)}{\mathrm{d}t}\int_0^a \frac{2\pi\epsilon_0 r\,\mathrm{d}r}{t_g - x(r,t)} \\ &= C_0\frac{\mathrm{d}V(t)}{\mathrm{d}t}\frac{\tanh^{-1}\left(\sqrt{x_p(t)/t_g}\right)}{\sqrt{x_p(t)/t_g}} \end{aligned} \tag{4.8}$$

As shown in Fig. 5.1, this is the sum of currents in C_0 and a nonlinear component i_c. Hence, the nonlinear part is

$$i_c(t) = C_0 \frac{\mathrm{d}V(t)}{\mathrm{d}t} \left[\frac{\tanh^{-1}\left(\sqrt{x_p(t)/t_g}\right)}{\sqrt{x_p(t)/t_g}} - 1 \right] \tag{4.9}$$

Taylor series expansion of i_c gives

$$i_c(t) \approx C_0 \frac{\mathrm{d}V(t)}{\mathrm{d}t} \left[\frac{1}{3}\left(\frac{x_p(t)}{t_g}\right) + \frac{1}{5}\left(\frac{x_p(t)}{t_g}\right)^2 \right] \tag{4.10}$$

To find the velocity current flowing through the clamped capacitance, the second term at the right hand side of (4.7) is rearranged and integrated over the membrane surface as $\delta r \to 0$

$$i_{vel}(t) = 2\pi\epsilon_0 V(t) \frac{\mathrm{d}x_p(t)}{\mathrm{d}t} \int_0^a \frac{(1 - r^2/a^2)^2 r \,\mathrm{d}r}{\left[t_g - x_p(t)(1 - r^2/a^2)^2\right]^2} \tag{4.11}$$

which is

$$i_{vel}(t) = \frac{C_0 V(t)}{2x_p(t)} \frac{\mathrm{d}x_p(t)}{\mathrm{d}t} \left[\frac{t_g}{t_g - x_p(t)} - \frac{\tanh^{-1}\sqrt{\frac{x_p(t)}{t_g}}}{\sqrt{\frac{x_p(t)}{t_g}}} \right] \tag{4.12}$$

Taylor series expansion of the velocity current expression is

$$i_{vel}(t) \approx \frac{C_0 V(t)}{t_g} \frac{\mathrm{d}x_p(t)}{\mathrm{d}t} \left[\frac{1}{3} + \frac{2}{5}\frac{x_p(t)}{t_g} + \frac{3}{7}\left(\frac{x_p(t)}{t_g}\right)^2 \right] \tag{4.13}$$

4.1 Small Signal Expressions

It is possible to obtain the small signal model parameters of the equivalent circuit from the Taylor series expansions of F_{tot}, i_c and i_{vel}. Assuming that the membrane displacement is very small compared to t_g around $x_p = 0$, we write from (4.6)

$$F_{tot}(t) \approx \frac{V^2(t) C_0}{2t_g} \left[1 + \frac{2x_p(t)}{3t_g} \right] \tag{4.14}$$

If we choose $V_{DC} \gg V_{ac}$, then $V^2(t) \approx V_{DC}^2 + 2V_{DC}V_{ac}(t)$ and since $x_{avg}(t) = x_p(t)/3$, we find

$$F_{tot}(t) \approx \frac{V_{DC}^2 C_0}{2t_g} + \frac{V_{DC} C_0}{t_g} V_{ac}(t) + \frac{V_{DC}^2 C_0}{t_g^2} x_{avg}(t) \tag{4.15}$$

where the first term at the right hand side represents the static force and the second term is the AC force due to electromechanical transformer ratio. The turns ratio of the transformer can be found from the second term as $N = V_{DC}C_0/t_g$ which is the same as that found in [1]. The third term in (4.15) is the amount of spring softening, due to increased electrostatic force caused by the displacement. It is like a negative capacitor of value $-C_0/N^2$ which is also consistent with [1].

For very small displacements around $x_p = 0$, the nonlinear part, i_c is negligible and the velocity current is

$$i_{vel}(t) \approx \frac{C_0 V_{DC}}{3t_g}\frac{\mathrm{d}x_p(t)}{\mathrm{d}t} = \frac{\sqrt{5}C_0 V_{DC}}{3t_g}v_{rms}(t) \tag{4.16}$$

The small signal parameters are sufficient to model a CMUT, as long as the membrane displacement is very small around $x_p = 0$ and the spring softening is not very pronounced. However, CMUTs are always used with DC bias and the assumption of operation around $x_p = 0$ is not realistic even under small signal AC conditions. Also, it is apparent, even from the linearized equations that the existence of large displacements can significantly alter the device behavior. In order to investigate the nonlinear nature of the CMUT, the unknown membrane displacement must be determined, so that the force and current equations can be implemented accordingly.

Chapter 5

Modeling of CMUT for Harmonic Balance Analysis

The harmonic balance (HB) analysis is a frequency domain nonlinear circuit analysis method, which is capable of finding the large signal, steady state response of nonlinear circuits and systems. Linear circuits are modelled in frequency domain, while nonlinear components are modelled with their time domain characteristics [21]. In this method, the input to the system is assumed to be a sinusoid and the steady state solution is found as the sum of a fundamental and its harmonics. The method is significantly more efficient than time-domain simulators when the circuit contains components that are modelled in the frequency domain and the time constants are large compared to the period of the fundamental excitation frequency. In [22], a harmonic balance approach is applied to the weakly nonlinear equations of a MEMS microphone, in order to characterize the unknown system parameters.

Transient FEM analysis shows that CMUT exhibits strong nonlinear behavior even at very low AC excitation and high DC bias. As seen in Fig. 5.1, we used

a linear mechanical section and a consistent radiation impedance. A commercial harmonic balance simulator[1] is utilized to implement the physical equations derived in Chapter 4. We also performed transient simulations in addition to harmonic balance simulations and compared the results with FEM simulations.

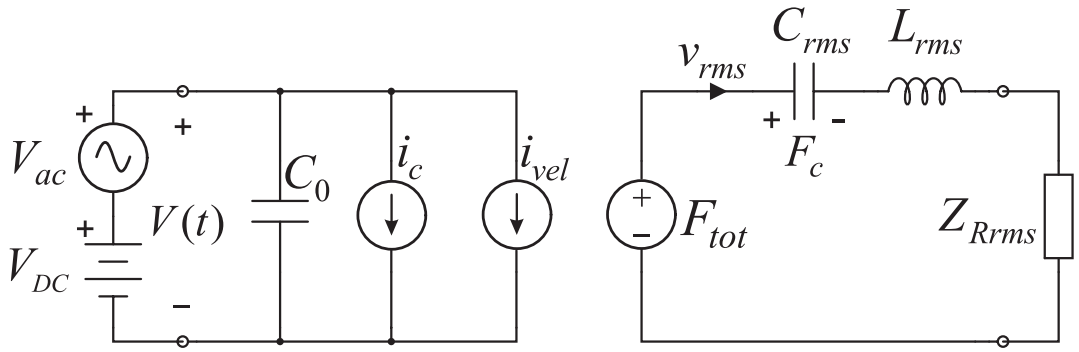

Figure 5.1: Nonlinear large signal equivalent circuit. i_c, i_{vel} and F_{tot} are given by (4.9), (4.12) and (4.4) with $x_p(t) = \sqrt{5}C_{rms}F_c(t)$. L_{rms} and C_{rms} are found by (3.6) and (3.7). Z_{Rrms} is given in the Appendix.

The mechanical section is constructed as lumped elements and a component that encapsulates the radiation impedance, $Z_{Rrms}(\omega)$, in the frequency domain with a suitable[2] file format. A symbolically-defined device in the HB simulator enables us to create, multi-port nonlinear equation based components. We implemented the physical equations of the CMUT by relating port currents, port voltages and their derivatives in this device. Equation (4.4) is used to generate the total force, F_{tot}, at the mechanical side of the equivalent circuit. Equations (4.9) and (4.12) give i_c and i_{vel} in the model of Fig. 5.1. $x_p(t)$ in those equations represents the instantaneous charge in C_{rms} and it can be found from $x_p(t) = \sqrt{5}C_{rms}F_c(t)$. For absolute peak membrane displacements of 0.1% of the gap height or less, Taylor expansions of the equations are used to avoid convergence problems that might occur for very small x_p values. We can calculate total power, total force and capacitive and velocity currents as outputs from the device. The actual circuit constructed in ADS is shown in Fig. 5.2.

[1]Advanced Design System (ADS), Agilent Technologies, www.agilent.com
[2]Touchstone formatted

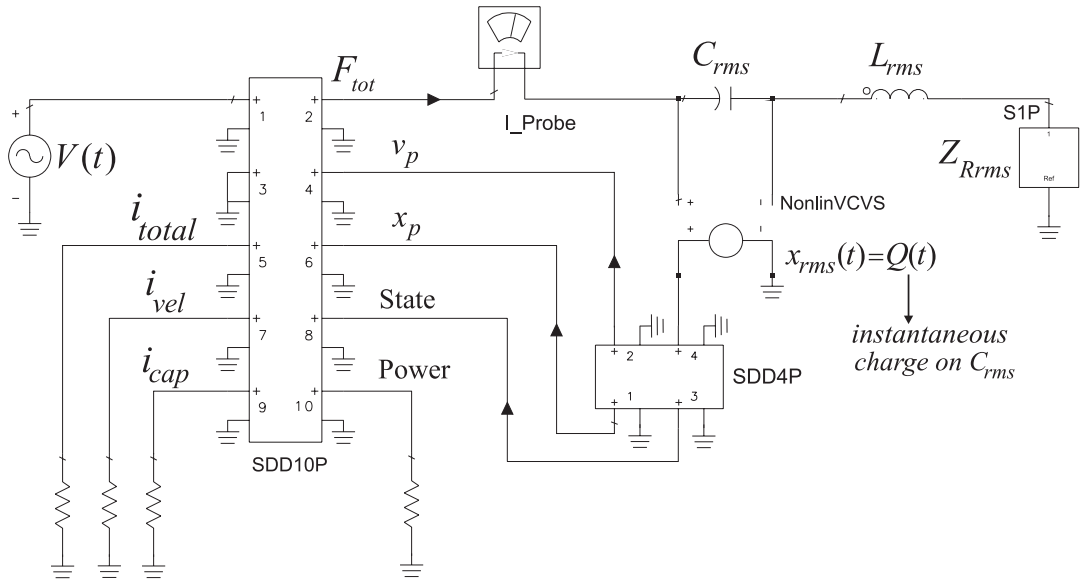

Figure 5.2: RMS equivalent circuit constructed in ADS.

5.1 Static Analysis

We compared the DC performance of the HB model with the FEM static analysis results. A CMUT membrane immersed in water with the top electrode placed at the bottom of the membrane is considered in all FEM simulations. Static deflection of a CMUT cell is examined with respect to DC bias voltage, the physical dimensions and the material properties of which are given in Table 5.1. The CMUT collapses at 95V in FEM analysis and at 97V in HB analysis, where $t_m/a = 0.05$. Moreover, increasing the thickness of the membrane, t_m, and repeating the analysis up to $t_m/a = 0.2$ revealed that the amount of error is confined within 3%. It must be noted that the choice of Mason's or rms mechanical section does not have any effect on the DC performance and the membrane displacement is determined by the force model employed. It is seen that the equivalent circuit predicts a higher peak displacement compared to FEM analysis.

The procedure is notably simplified while deriving the mechanical impedance of the CMUT with the assumption of constant force distribution in (3.5). The

across variable is simply defined as total force on the membrane, F_{tot}, consistent with the phasor notation. However, there is an effect of nonuniform force distribution which becomes significant particularly when the membrane is biased close to the collapse point. FEM analysis reveals that the force distribution is effectively uniform under low bias conditions and a nonuniform component emerges as the bias is increased and becomes significant at high bias levels. This phenomenon is seen in Fig. 5.3, where the force along the driven surface of the membrane is retrieved from 80 discrete radial positions and divided by the ring area ($2\pi r\,\delta r$) that it acts on. 1V peak AC excitation voltage is applied on 40V and 85V bias voltages for comparison. Results are obtained from FEM transient analysis and subsequently processed in MATLAB. DC and fundamental AC magnitudes of the profile are acquired from the discrete fourier transform (*fft* command in MATLAB) of the force data at each 80 location and plotted on two separate graphs. The left y-axis and right y-axis corresponds to the result obtained for 40V and 85V bias voltage, respectively. For a fair comparison, these y-axes are arranged such that, the whole range seen on each axis divided by the mean of the profile of each bias case are equal. In this way, non-uniformity of force over area profile on the strongly biased membrane is more evident than the less biased one. As seen in Fig. 5.3, profile of the force distribution across the membrane has two superimposed components. The dominant contribution is a uniform force distribution, while an additive force profile similar to velocity distribution is present. In fact, as we observed from transient FEM analyses, this behavior is not limited to DC force distribution, but it is similar for AC components of the force as well.

FEM simulations show that force is larger at the center of the membrane compared to its periphery. We used the total force on the membrane as the lumped across variable in the model, which estimates a lower deflection at the center. When the force distribution is significantly nonuniform, we can consider the rms force along the membrane radius, F_{rms}, as the across variable in the

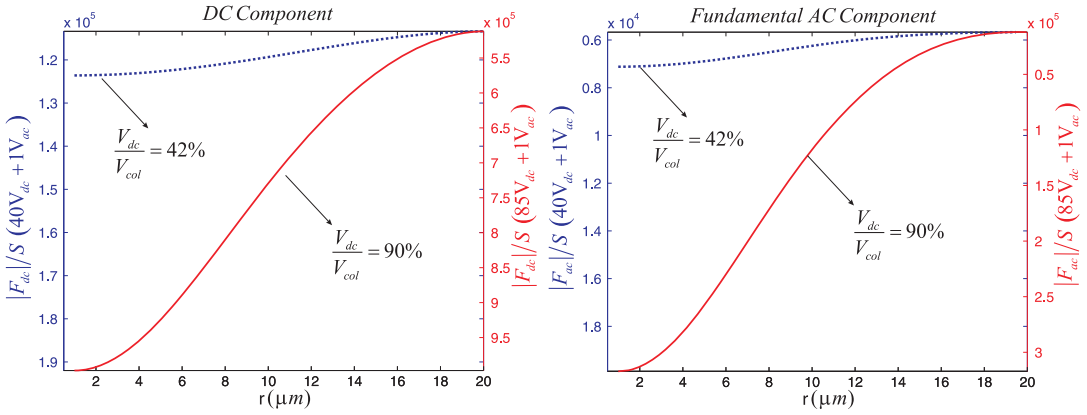

(a) (b)

Figure 5.3: FEM transient analysis results for (a) DC and (b) fundamental AC components of the force over area (S) profile at the driven surface of the CMUT, for two different bias conditions.

model. Analytical justification of replacing F_{tot} by F_{rms} is not readily available, but can be made in an *ad hoc* manner, based on the argument that F_{rms} represents the acting force more accurately. The CMUT collapses at $95V$ in FEM analysis, where it collapses at $92V$ and 97 in HB analysis, when F_{rms} and F_{tot} is considered, respectively. Root mean square force across the driven surface of the membrane can be defined as,

$$F_{rms} = \pi a^2 \sqrt{\frac{1}{\pi a^2} \int_0^{2\pi} \int_0^{a} p^2(r) r \mathrm{d}r \mathrm{d}\theta} \tag{5.1}$$

where $p(r)$ is again the normal force distribution.

Equation 5.1 can be evaluated for $n = 2$ as follows

$$F_{rms} = \frac{1}{2} V^2(t) \frac{C_0}{t_g} \left\{ \frac{15\left(\frac{x_p(t)}{t_g}\right)^2 - 40\left(\frac{x_p(t)}{t_g}\right) + 33}{48\left(1 - \frac{x_p(t)}{t_g}\right)^3} + \frac{5}{16} \frac{\tanh^{-1}\left(\sqrt{\frac{x_p(t)}{t_g}}\right)}{\sqrt{\frac{x_p(t)}{t_g}}} \right\}^{1/2} \tag{5.2}$$

Taylor series expansion of F_{rms} gives

$$F_{rms} \approx \frac{V^2(t) C_0}{2 t_g} \left[1 + \frac{2}{3} \frac{x_p(t)}{t_g} + \frac{7}{9} \left(\frac{x_p(t)}{t_g} \right)^2 \right] \tag{5.3}$$

Table 5.1: CMUT dimensions and constant parameters used in the simulations.

Parameter	Value
Radius, a	20μm
Gap Height, t_g	0.25μm
Thickness of membrane, t_m	1μm
Collapse voltage, V_{col}	95V
Poisson's Ratio of Si_3N_4, σ	0.263
Density of membrance (Si_3N_4), ρ	3.27 g/cm^3
Young's modulus of Si_3N_4, Y_0	3.2×10^5 MPa
Density of water, ρ_0	1 g/cm^3
Speed of sound in water, c	1500 m/sec

Mechanical section of the rms equivalent circuit for this new configuration is achieved by changing the applied force at the mechanical side of the equivalent circuit:

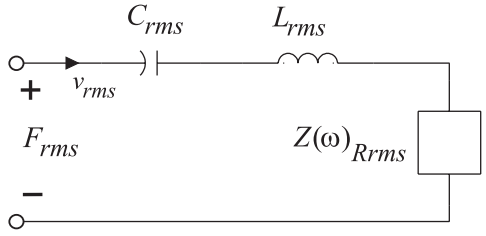

Figure 5.4: Mechanical section of the rms circuit, where F_{tot} is replaced by F_{rms}.

5.2 Frequency Response Analysis

5.2.1 Small-Signal Analysis

A prestressed harmonic analysis in FEM is used to calculate the dynamic response of a biased membrane, assuming that the harmonically varying stresses are much smaller than the prestress itself. This analysis does not take into account any kind of nonlinearity. Therefore, it is meaningful to evaluate only the small signal frequency response, where the membrane should not be biased close to the collapse point. We can define the transducer's electrical admittance as $Y_{in} = G_{in} + jB_{in}$, where G_{in} is the conductance and B_{in} is the susceptance of the

CMUT. In order to follow the progress made in rms equivalent circuit approach, first, Mason's mechanical section is analyzed in the harmonic balance simulator. LC parameters in [4] and the analytically calculated radiation impedance of a clamped membrane, $Z_{Ravg}(\omega)$, in [18] are used. F_{tot} and v_{avg} are utilized while implementing (4.4), (4.9) and (4.12) in the circuit. By using this model, small signal electrical conductance of an immersed CMUT cell is found and compared with the FEM harmonic analysis result. The model with Mason's mechanical section predicts resonance frequencies of 6.5, 6.35 and 6.2 MHz as seen in Fig. 5.5, for the bias voltages of 60V, 70V and 80V, respectively. However, FEM harmonic analysis yields resonance frequencies of 4.94, 4.75 and 4.47 MHz for the same bias voltages. With an applied AC signal of 1V peak on top of $\mathrm{V}_{DC} = 90\mathrm{V}$, the membrane collapses around the resonance frequency. As expected, due to the spring softening effect, the resonance shifts to a lower frequency as the bias voltage is increased. The spring softening is more pronounced in the FEM analysis, the resonance frequencies are significantly lower and the magnitudes are higher, compared to the equivalent circuit constructed by Masons's mechanical section. Hence, as the plots show, using Mason's average velocity model for an immersed CMUT is inadequate.

Improvement is obtained when Mason's equivalent mechanical section and the corresponding radiation impedance is replaced by the rms equivalent mechanical section, L_{rms} and C_{rms}, and the respective radiation impedance, Z_{Rrms}, as explained in Section 3.3. In this circuit, root mean square velocity, v_{rms} and F_{tot} are the through and across variables, respectively. The conductance obtained by this model for the same bias levels is depicted in Fig. 5.6 together with the FEM results. Much better agreement is achieved compared to the model constructed by using Mason's mechanical section, in terms of peak conductance level and resonance frequency estimation. The spring softening is also better estimated in the rms equivalent circuit. However the amplitude of the conductance and the resonance frequency is a little higher and the quality factor is lower in HB results

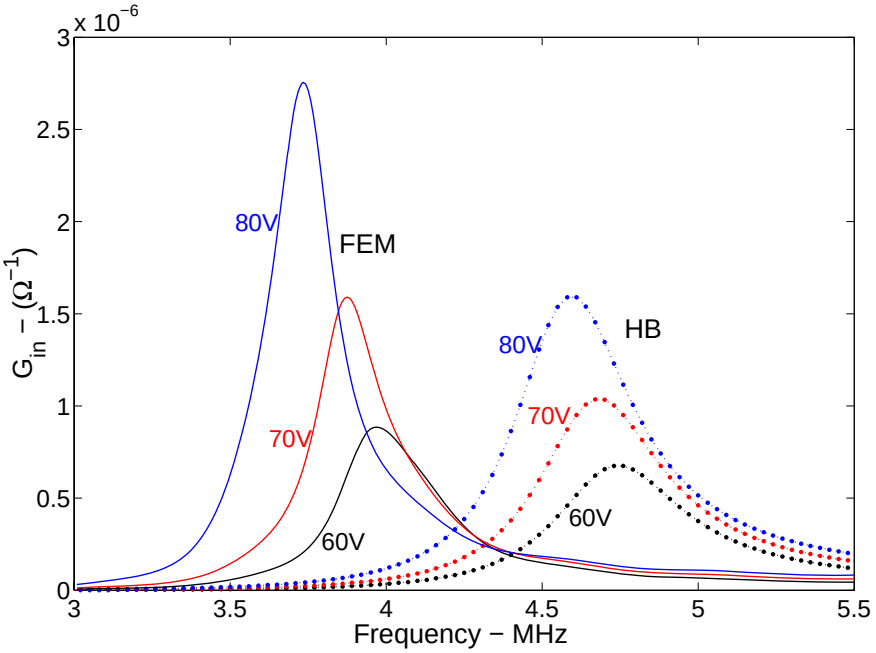

Figure 5.5: Small signal electrical conductance, G_{in}, of the CMUT cell in water under various bias voltages. 1V peak AC signal is applied. FEM (solid) results are acquired from prestressed harmonic analysis. Nonlinear rms equivalent circuit frequency response is obtained from HB (dotted) simulations, by implementing F_{tot} and v_{avg} definition.

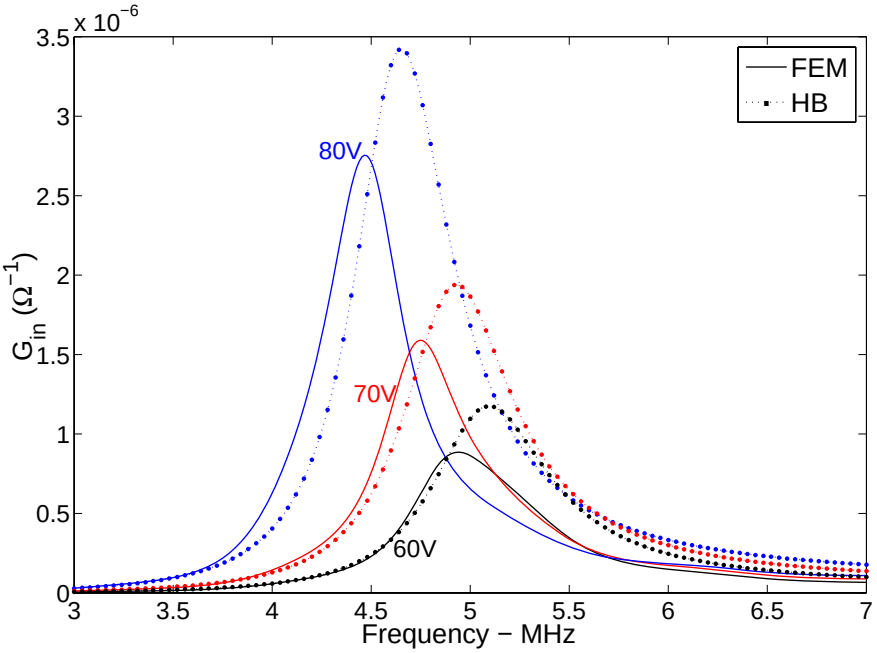

Figure 5.6: Small signal electrical conductance, G_{in}, of the CMUT cell in water under various bias voltages. 1V peak AC signal is applied. FEM (solid) results are acquired from prestressed harmonic analysis. Nonlinear rms equivalent circuit frequency response is obtained from HB (dotted) simulations, by implementing F_{tot} and v_{rms} definition.

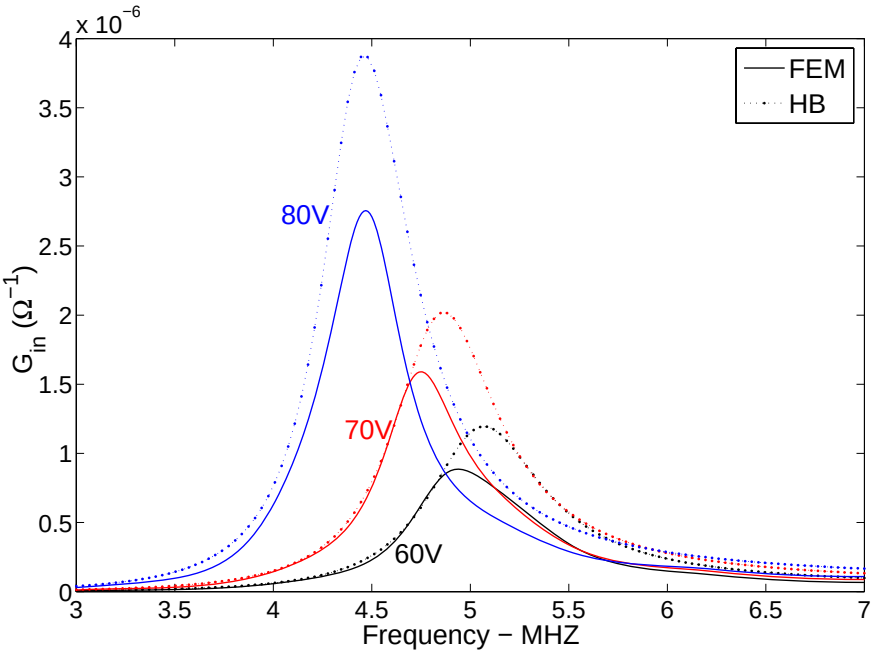

Figure 5.7: Small signal electrical conductance, G_{in}, of the CMUT cell in water under various bias voltages. 1V peak AC signal is applied. FEM (solid) results are acquired from prestressed harmonic analysis. Nonlinear rms equivalent circuit frequency response is obtained from HB (dotted) simulations, by implementing F_{rms} and v_{rms} definition.

compared to FEM. We can see that the resonance frequency shift due to increased bias voltage falls short as the bias voltage increases, where the nonuniform force distribution begins to be significant and the clamped membrane velocity profile changes (n increases). These two major variations increase the error rate as we approach close to the collapse point.

We noted that under high bias conditions nonuniform component of force distribution becomes significant. We replaced the across variable F_{tot} by F_{rms} in the rms circuit and used the mechanical section depicted in Fig. 5.4. The predictions of this circuit is given in Fig. 5.7. The model successfully predicts the resonance frequency with significantly reduced error.

We observed similar results for CMUTs having the same radii but thicker membranes up to $t_m/a = 0.2$. Small signal electrical conductance of immersed CMUT cells with 20μm radius and various thicknesses is depicted in Fig. 5.8.

80% and 0.1% of the collapse voltage of each CMUT is applied as the bias and peak AC voltage, respectively. Keeping the radius of the CMUT constant as the membrane gets thicker, resonance frequency shifts to a higher frequency, membrane compliance (C_{rms}) decreases and ka increases. Notice that, in Fig. 3.2, radiation resistance of a clamped membrane increases up to $ka = 4$, which consequently decreases the quality factor of the CMUT cell as the membrane thickness increases. This is demonstrated in Fig. 5.8.

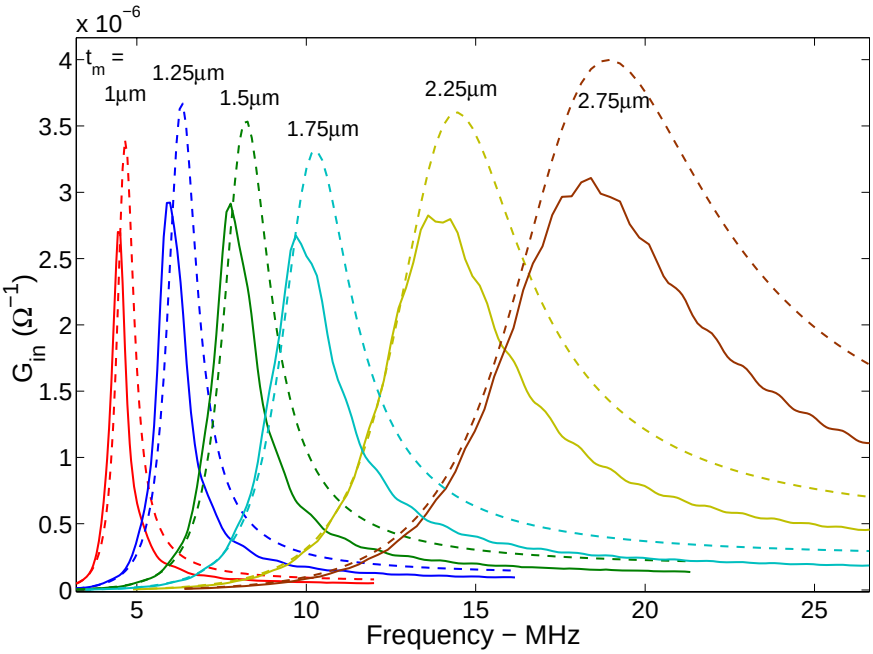

Figure 5.8: Small signal electrical conductance, G_{in}, of CMUT cells in water for various thicknesses and $a = 20\mu$m. FEM (solid) results are acquired from prestressed harmonic analysis. Nonlinear rms equivalent circuit frequency response is obtained from HB (dashed) simulations, by implementing F_{tot} and v_{rms} definition.

We have also carried out the transient FEM analysis at several discrete frequencies, to validate the linear behavior of the membrane under these drive conditions. We observed that the transient analysis yields exactly same results with the prestressed harmonic analysis in FEM for linear operations.

5.2.2 Nonlinear Analysis

Prestressed harmonic analysis is reliable for small signal simulations. In order to find out the large signal performance of the introduced model, we employed dynamic transient analysis in FEM, both for large V_{ac} and for small V_{ac} when the membrane operates near the collapse region. In Fig. 5.9, the real part of the fundamental component of the source current is shown for HB analysis, together with transient and prestressed harmonic FEM analyses. In these simulations V_{DC} and V_{ac} are 10V and 40V peak, respectively. There is a peak at half the res-

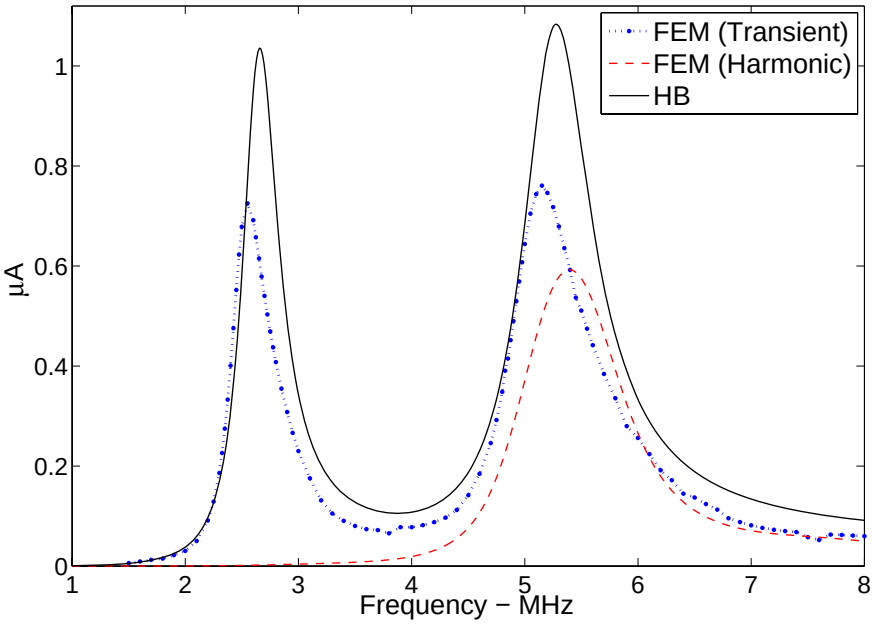

Figure 5.9: Real part of the fundamental electrical source current of the CMUT cell in water for $V_{DC} = 10$V and a peak AC voltage of 40V. Large signal response is examined in FEM, both with transient (dotted) and prestressed harmonic analysis (dashed). RMS equivalent circuit result is obtained from HB (solid) simulation.

onance frequency, since the second harmonic coincides the resonance frequency causing significant membrane velocity at the resonance. However, prestressed FEM harmonic analysis fails to predict the nonlinear behavior. On the other hand, the rms equivalent circuit predicts the conduction peak at half the resonance frequency quite well. The data of the equivalent circuit for this figure is

obtained in less than one minute, while producing the data of transient FEM analysis took approximately one day on the same computer.

Total Harmonic Distortion

The sum of all undesired harmonic energy at the generated force, F_{tot}, and the radiating output pressure signal, can be expressed as a percentage of the corresponding fundamental component. We calculated the total harmonic distortion (THD) from,

$$THD = 100\frac{\sqrt{V_2^2 + V_3^2 + \cdots + V_m^2}}{V_1} \tag{5.4}$$

where V_m is the rms voltage of harmonic m and m=1 is the fundamental harmonic. Using the equivalent circuit model, THD is calculated with respect to

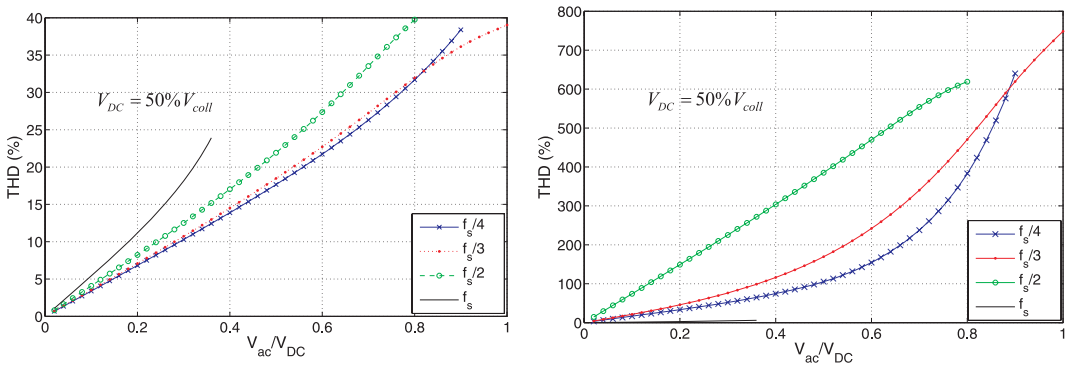

(a) (b)

Figure 5.10: (a) Total harmonic distortion (THD) percentage at F_{tot} and (b) at the radiating acoustic signal when the bias is 50% of the collapse voltage and the excitation frequency less than or equal to the series resonance frequency (f_s).

V_{ac}/V_{DC} at different excitation frequencies. Total harmonic distortion at F_{tot} and the radiating acoustic signal are depicted in Fig. 5.10 and Fig. 5.11, for bias voltages of 50% and 80% of the collapse voltage, V_{coll}, respectively. Excitation frequency is less than or equal to the series resonance frequency (f_s). In the equivalent circuit considered, acoustic signal radiating to the medium is the voltage drop on the radiation impedance. In the figures, V_{ac} is increased until the membrane collapses at the specified frequency of operation. Notice that, model

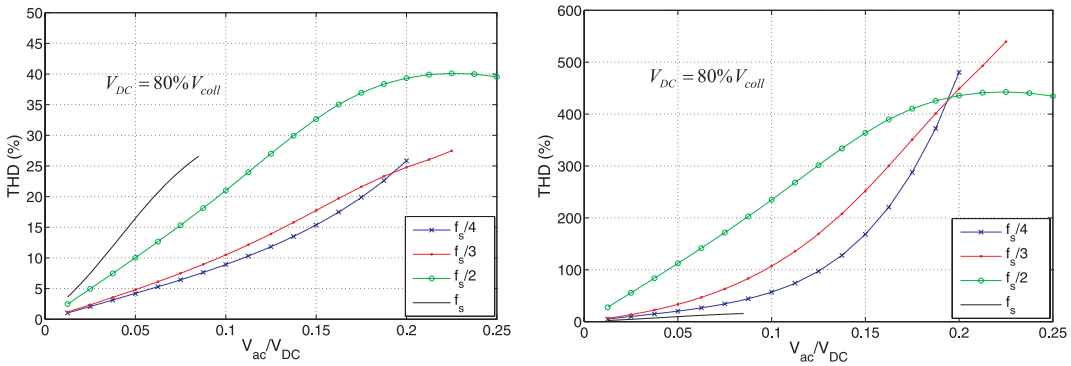

Figure 5.11: (a) Total harmonic distortion (THD) percentage at F_{tot} and (b) at the radiating acoustic signal when the bias is 80% of the collapse voltage and the excitation frequency less than or equal to the series resonance frequency (f_s).

prediction is accurate up to more than two times the series resonance frequency, which reveals that investigation of the harmonic distortion is meaningful only when harmonics appear in the valid operation region. For instance, when the frequency is $f_s/4$, THD calculated in Fig. 5.10 and Fig. 5.11 is accurate even when the ninth harmonic is significantly present. On the other hand, when the applied frequency is f_s, solely the second harmonic must be taken into consideration since the third harmonic is already beyond the operation region of the model. However, we observed that at frequency f_s, the contribution of the second harmonic to the total harmonic distortion is more than 90% of the sum of all other harmonics except the fundamental harmonic. According to this argument, evaluation of harmonic distortion by using the model is achievable up to frequency f_s.

5.3 Transient Analysis

In Fig. 5.12, the displacement at the center of the membrane is plotted, which is driven with a sinusoidal signal of 50V peak amplitude at 1 MHz, superimposed

on 40V bias voltage. The drive frequency is approximately one fifth the resonance frequency of CMUT cell. HB solution converges within one second, which approximates the steady state of a transient FEM solution accurately. Nonlinear effects are very pronounced, since a large AC signal is employed. Other FEM transient and HB simulation results are also included in the Appendix B.

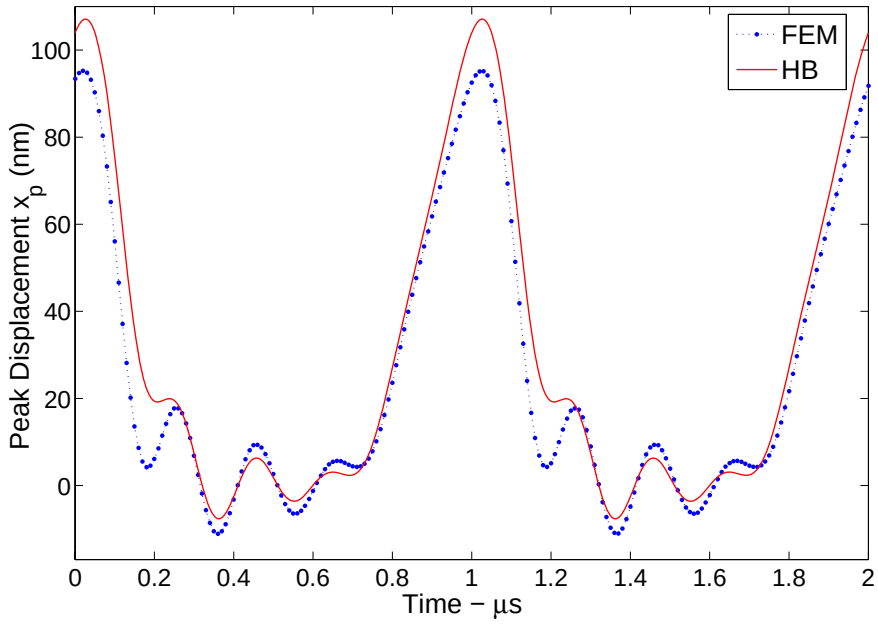

Figure 5.12: Peak displacement of the CMUT cell in water, which is driven with a high sinusoidal voltage at a frequency of one fifth the resonance. Comparison between transient analysis in FEM (dotted) and HB (solid) simulation of the nonlinear rms equivalent circuit.

Although, the harmonic balance simulates the nonlinear circuits rapidly, it only produces the steady state response. We also studied the transient effects of the same rms equivalent circuit by means of transient simulations. Fig. 5.13 shows the peak displacement of the membrane, where the membrane is biased to 40 volts and a rectangular pulse of 40 volts amplitude is superimposed for $0.1\mu s$ duration. Although the agreement is impressive, FEM simulation predicts a slightly faster damping.

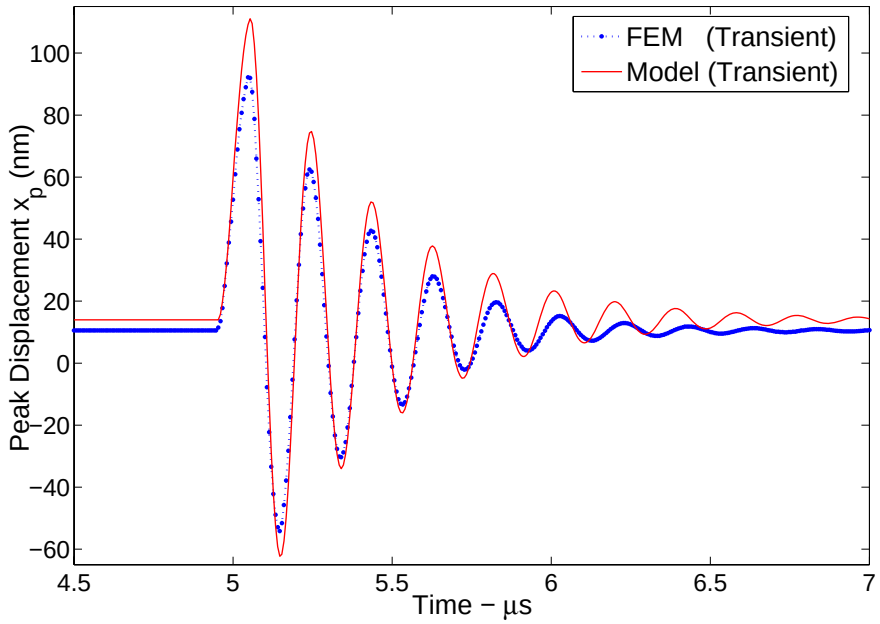

Figure 5.13: Peak displacement of the CMUT cell in water, which is driven with a $0.1\mu s$ pulse. $V_{low} = 40V$, $V_{high} = 80V$. Comparison between the transient analyses carried out both in FEM (dotted) and the nonlinear rms equivalent circuit (solid) are shown.

5.4 Pulse Shaping

Utilizing the equivalent model equations and parameters, we can design the shape of the driving voltage in order to obtain the desired acoustic signal. A pressure pulse, which has a Gaussian shaped frequency spectrum, is an appropriate choice at the surface of the membrane. The procedure is demonstrated in Fig. 5.14. First, the magnitude, the bandwidth and the center of this spectrum is determined. Then, the rms velocity is found in the frequency domain, from the ratio of the desired total force at the top surface of the membrane and the impedance of the medium. The total force, F_{tot}, at the driven surface is calculated in the frequency domain from the product of rms velocity and the total mechanical impedance and then inverse Fourier transformed. Finally, the driving voltage is calculated from (4.4).

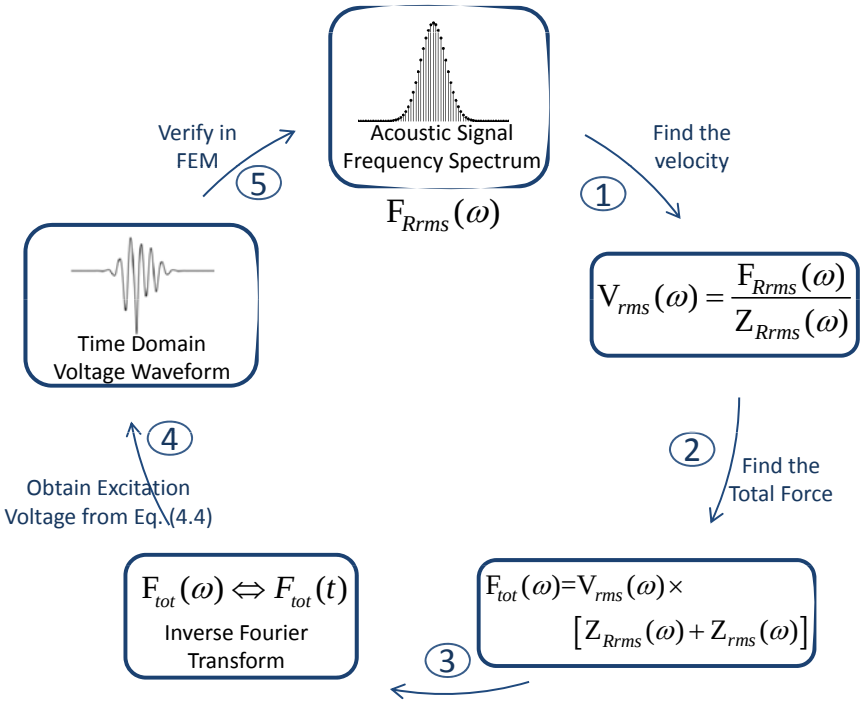

Figure 5.14: Pulse Shaping Process.

If the desired pulse across the radiation impedance is as shown in Fig. 5.15(a), the model predicts the driving voltage as given in Fig. 5.15(b). In order to verify its validity, FEM transient analysis is done using this driving voltage and the obtained result is plotted in Fig. 5.15(a). The obtained pulse shape is a little distorted compared to the expected one. However, the results are very similar both in FEM and HB. We note that calculating the driving voltage and obtaining the result in HB takes place in less than one minute. Although the frequency spectrum of the desired pulse is centered at 3 MHz with a 6-dB bandwidth of 1.2 MHz, the necessary drive voltage contains significant harmonics nearly up to 12 MHz as evident from its frequency spectrum shown in Fig. 5.15(c). If a larger bandwidth is aimed centered at the resonance frequency, even more harmonics are needed at higher frequencies for the excitation voltage. The linear mechanical LC section is valid over a wide frequency band around the resonance frequency, but it fails to represent the membrane dynamics as the frequency approaches to anti resonance. For instance, beyond about 14 MHz, the model of the CMUT being analyzed is not valid, since the velocity profile no more

resembles to the clamped membrane velocity profile. The anti-resonance of this particular immersed membrane is around 25 MHz. As long as the frequency spectrum of the obtained driving voltage is confined in the valid operation band of the model, the obtained pulse shape will be very similar to the desired one.

As another example, assume that we want to obtain the desired pulse shown in Fig. 5.16(a), which has a frequency spectrum centered near the resonance frequency, at 6 MHz. The fractional bandwidth of the desired pulse is the same as before. This time, by using the model equations and parameters, we calculate the voltage waveform in Fig. 5.16(b). Notice that, as seen in Fig. 5.16(c), the frequency spectrum of the designed voltage waveform contains irrelevant harmonics beyond the valid operation region. As a result, verification of this design shows that the FEM result in Fig. 5.16(a) contains oscillations at the end of the pulse.

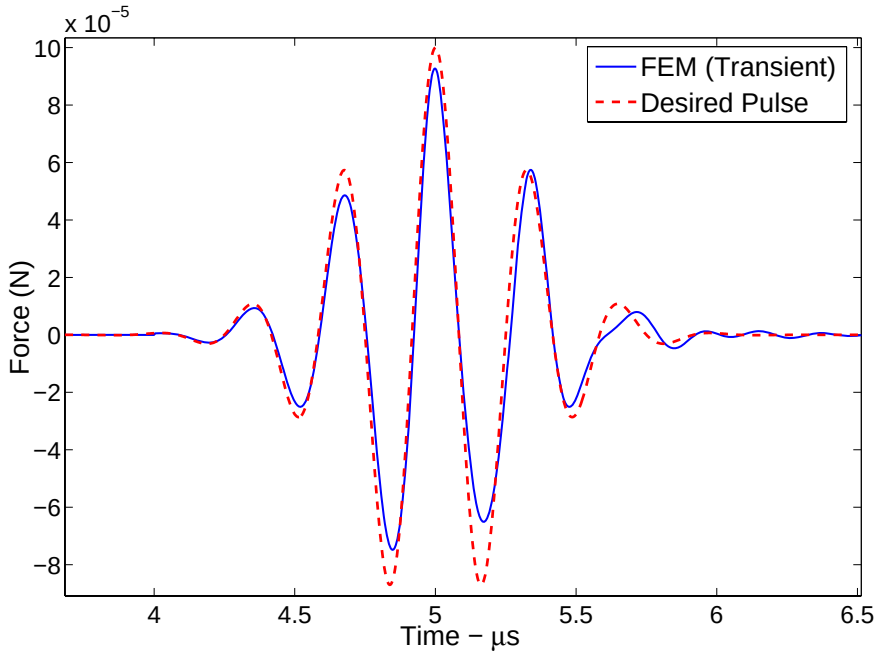

(a)

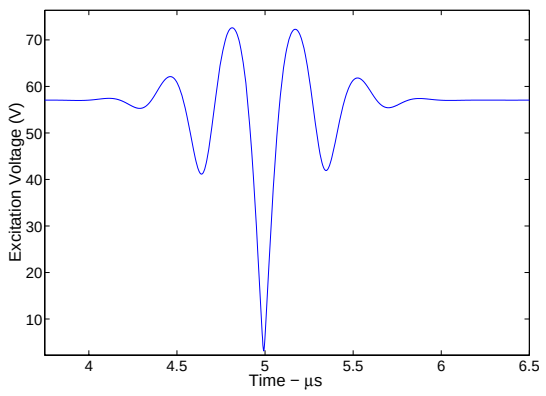

(b)

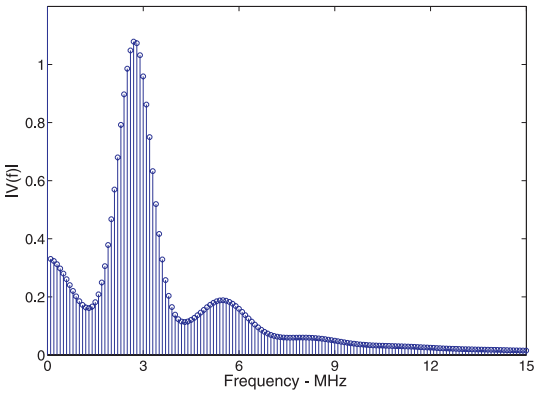

(c)

Figure 5.15: (a) The desired pulse shape (dashed) and the achieved total force (solid) at the top surface of the CMUT in water, which is obtained when the designed voltage waveform in (b) is applied in FEM transient analysis. (c) The frequency spectrum of the voltage waveform.

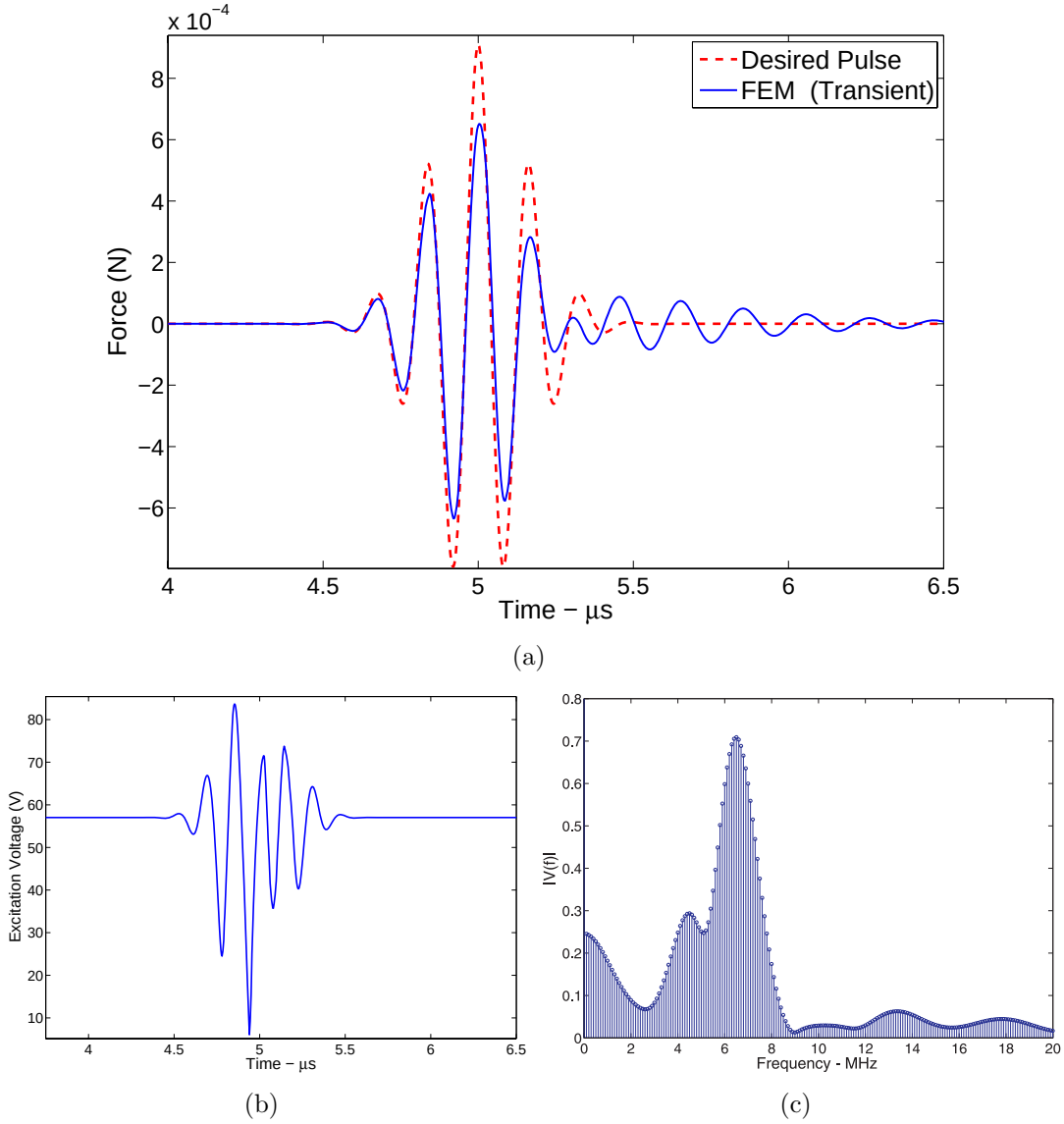

Figure 5.16: (a) The desired pulse shape (dashed) and the achieved total force (solid) at the top surface of the CMUT in water, which is obtained when the designed voltage waveform in (b) is applied in FEM transient analysis. (c) The frequency spectrum of the voltage waveform.

Chapter 6

Conclusions

An alternative equivalent circuit for immersed transmitting circular CMUT is presented for linear and nonlinear operations. Root mean square velocity is used instead of the commonly used average velocity. A clamped profile is utilized when deriving the analytical force and current equations and the corresponding radiation impedance is employed. Everything in the model can be simply calculated analytically for particular device dimensions, independent of FEM analysis. Although, there is no parameter tuning in our model using the FEM results, the predictions are accurate.

In Mason's equivalent circuit model the through variable is the average velocity along the membrane surface and the inductance representing the mass of the membrane is 1.8 times the membrane mass. However, the model can preserve the kinetic energy of the membrane mass only if the root mean square velocity is used as the through variable. When rms velocity is employed in the model $L_{rms} = L_M/1.8$ and $C_{rms} = 1.8C_M$, where L_M and C_M constitute the LC section of Mason's circuit. Therefore, the series resonance frequency in vacuum is independent of the choice v_{avg} or v_{rms} and the prediction is accurate. However, when the CMUT is immersed, resonance frequency prediction is only accurate when

the model employs the rms LC section, which is terminated with the consistent radiation impedance, Z_{Rrms}.

The radiation impedance of a transducer depends on the particle velocity distribution across its aperture. It is shown that radiation impedance of a piston transducer and a clamped membrane are considerably different, which indicates that piston models are not appropriate for immersed CMUT models.

Differences between the FEM results and the model predictions can be accounted for the approximations in the model equations. One of them is the variable nature of n as a function of bias voltage. We made use of FEM transient analysis and attained the velocity profile of each significant harmonic. We observed that the membrane deflection profile can be modelled quite accurately by (3.1) for n varying between 1.95 and 2.25. We have taken n=2, which corresponds to clamped membrane velocity profile and derived the model equations. The stress stiffening effect is also neglected in the linear mechanical section, which may be pronounced when large deflections occur. However, a correction for the stiffness of the membrane (C_{rms}) is employed according to device dimensions.

The force distribution across the membrane is not uniform. FEM simulations show that force is larger at the center of the membrane compared to its periphery. We used the total force on the membrane as the lumped across variable in the model, which estimates a lower deflection at the center. Although, F_{rms} is utilized to include the pressure distribution effect on the membrane, recalculation of the mechanical membrane impedance, Z_{rms}, might also be taken into consideration for nonuniform pressure distribution.

In general, the model is easy to use, intuitive and very rapid compared to FEM, which makes it useful for design purposes such as pulse shaping. Although, the operation region of the model is restricted, it is sufficient for many cases. As a future work, it is aimed to extend the valid operation region and to use this

model for designing an array of CMUTs by taking into account the effect of mutual impedance between the array cells.

APPENDIX A

Radiation Impedance

Radiation impedance of a transducer with a certain velocity profile is the ratio of total power radiated from the acoustical terminals to the square of the absolute value of a nonzero reference velocity:

$$Z_R = \frac{2\pi \int_0^a P(r)v^*(r)r\,\mathrm{d}r}{V_i V_i^*} = \frac{P_{TOTAL}}{|V_i|^2} \tag{A.1}$$

When rms velocity is chosen for V_i, the radiation impedance derived in [18] becomes

$$Z_{Rrms} = \pi a^2 \rho_0 c \left(1 - \frac{20}{(ka)^9}\left[F_1(2ka) + jF_2(2ka)\right]\right) \tag{A.2}$$

where ρ_0 is the density and c is the speed of sound of the immersion medium and

$$\begin{aligned} F_1(y) =& (y^4 - 91y^2 + 504)J_1(y) \\ &+ 14y(y^2 - 18)J_0(y) - y^5/16 - y^7/768 \end{aligned} \tag{A.3}$$

and

$$\begin{aligned} F_2(y) =& -(y^4 - 91y^2 + 504)H_1(y) \\ &- 14y(y^2 - 18)H_0(y) + 14y^4/15\pi - 168y^2/\pi \end{aligned} \tag{A.4}$$

J_n and H_n are the nth order Bessel and Struve functions, respectively.

For $ka < 0.1$, $Z_{Rrms} = R_{Rrms} + jX_{Rrms}$ can be approximated as

$$Z_{Rrms} \approx \frac{5}{9}\pi a^2 \rho_0 c \left[\frac{(ka)^2}{2} + j\frac{2^{16}}{17325\pi}(ka)\right] \tag{A.5}$$

APPENDIX B

FEM Transient and HB Analysis Results

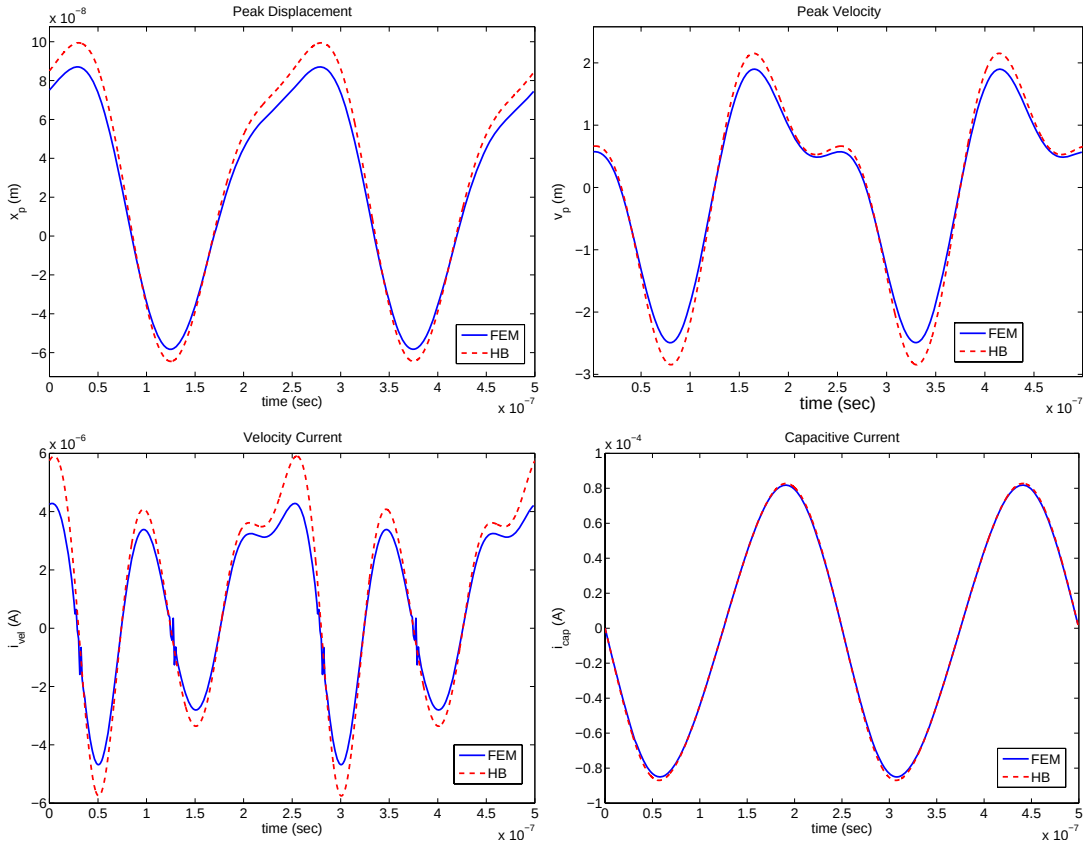

Figure B.1: FEM transient and HB analysis results obtained for $a = 20\mu m, t_g = 0.25\mu m, t_m = 1\mu m$. Excitation voltage is $V_{dc} = 60V, V_{ac} = 70V at f = 4MHz$.

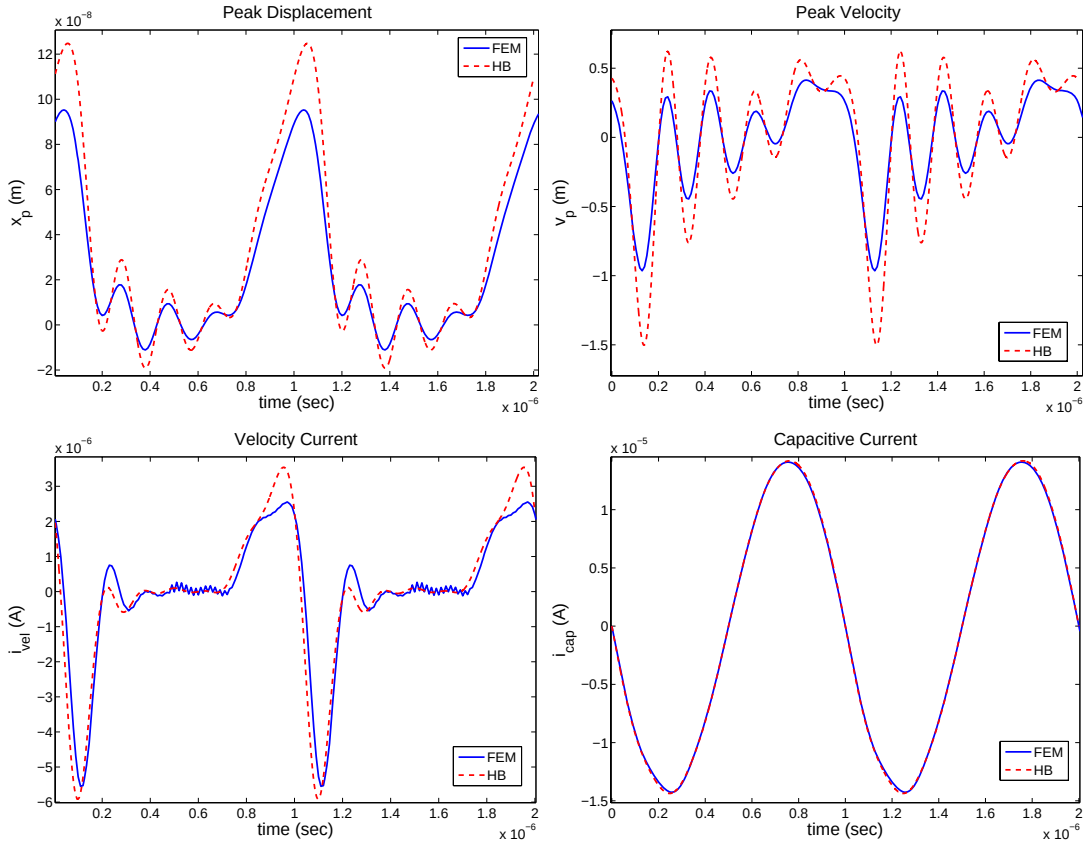

Figure B.2: FEM transient and HB analysis results obtained for $a = 20\mu m, t_g = 0.25\mu m, t_m = 1\mu m$. Excitation voltage is $V_{dc} = 40V, V_{ac} = 50V at f = 1MHz$.

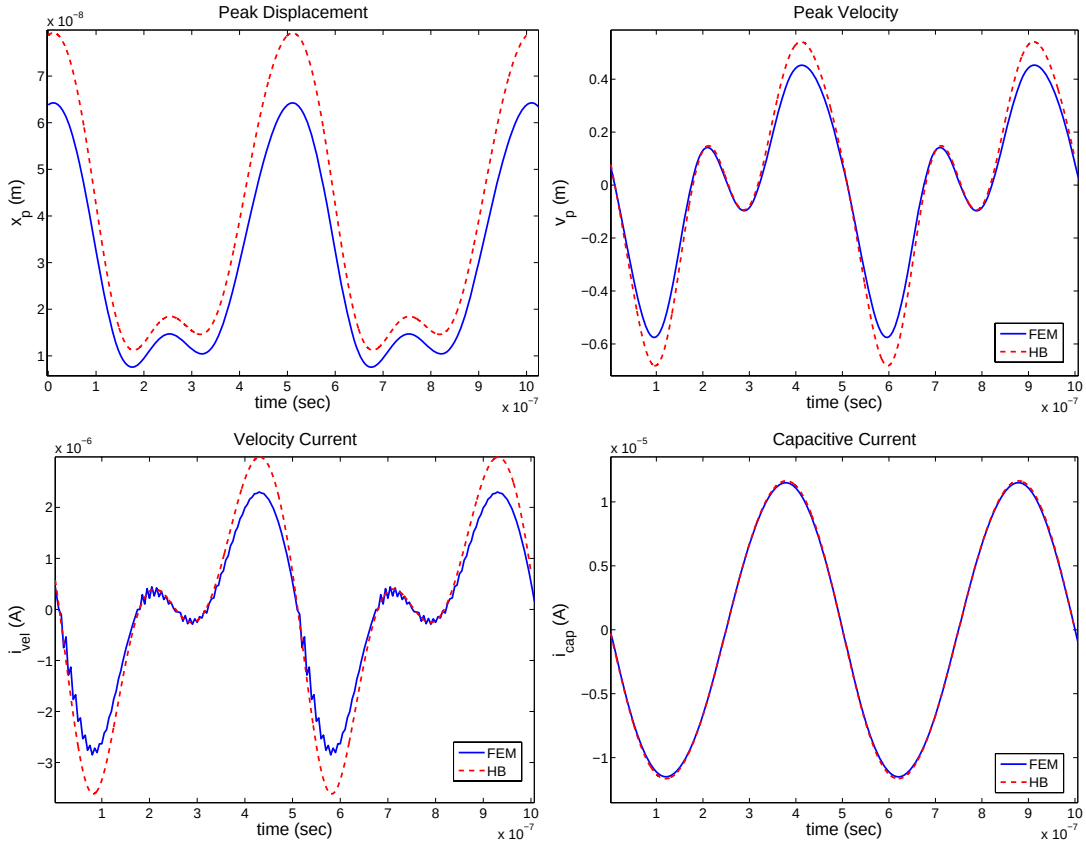

Figure B.3: FEM transient and HB analysis results obtained for $a = 20\mu m, t_g = 0.25\mu m, t_m = 1\mu m$. Excitation voltage is $V_{dc} = 60V, V_{ac} = 20V at f = 2MHz$.

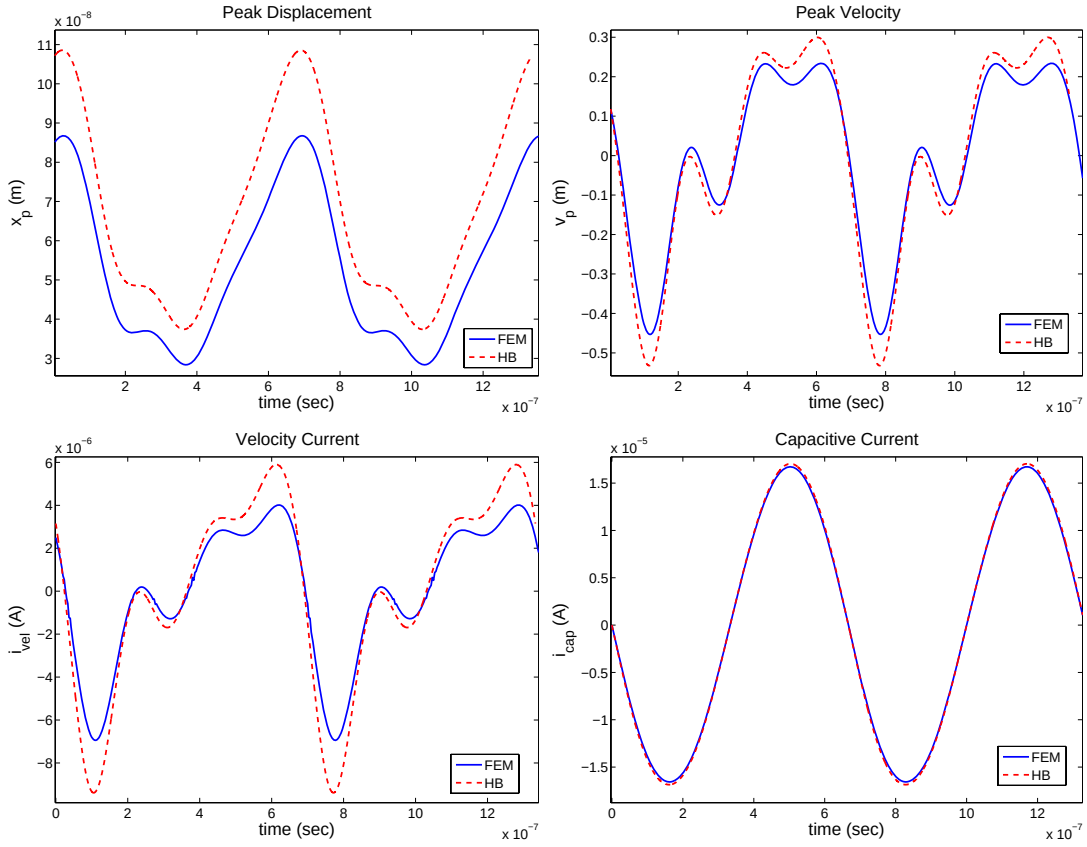

Figure B.4: FEM transient and HB analysis results obtained for $a = 30\mu m, t_g = 0.3\mu m, t_m = 2\mu m$. Excitation voltage is $V_{dc} = 120V, V_{ac} = 20V at f = 1.5MHz$.

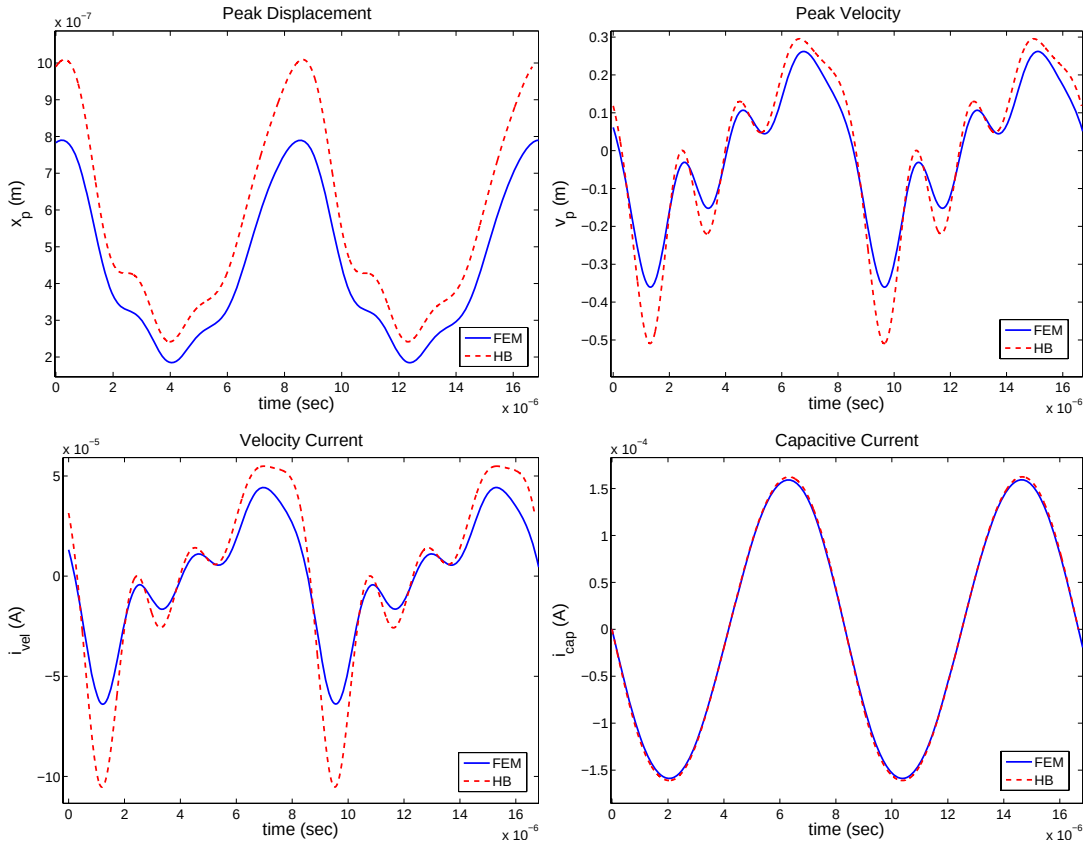

Figure B.5: FEM transient and HB analysis results obtained for $a = 300\mu m, t_g = 2.5\mu m, t_m = 20\mu m$. Excitation voltage is $V_{dc} = 900V, V_{ac} = 200V at f = 0.12MHz$.

Bibliography

[1] I. Ladabaum, X. Jin, H. Soh, A. Atalar, and B. Khuri-Yakub, "Surface micromachined capacitive ultrasonic transducers," *IEEE Trans. on Ultrason., Ferroelec. and Freq. Cont.*, vol. 45, no. 3, pp. 678–690, May 1998.

[2] J. Knight, J. McLean, and F. Degertekin, "Low temperature fabrication of immersion capacitive micromachined ultrasonic transducers on silicon and dielectric substrates," *IEEE Trans. on Ultrason., Ferroelec. and Freq. Cont.*, vol. 51, no. 10, pp. 1324–1333, Oct. 2004.

[3] Y. Huang, A. Ergun, E. Haeggstrom, M. Badi, and B. Khuri-Yakub, "Fabricating capacitive micromachined ultrasonic transducers with wafer-bonding technology," *J. Microelectromech. Syst.*, vol. 12, no. 2, pp. 128–137, Apr 2003.

[4] W. Mason, *Electromechanical Transducers and Wave Filters. 2nd ed.* Van Nostrand, New York, 1948.

[5] H. Koymen, M. Senlik, A. Atalar, and S. Olcum, "Parametric linear modeling of circular cMUT membranes in vacuum," *IEEE Trans. on Ultrason., Ferroelec. and Freq. Cont.*, vol. 54, no. 6, pp. 1229–1239, June 2007.

[6] A. Lohfink and P.-C. Eccardt, "Linear and nonlinear equivalent circuit modeling of CMUTs," *IEEE Trans. on Ultrason., Ferroelec. and Freq. Cont.*, vol. 52, no. 12, pp. 2163–2172, Dec. 2005.

[7] D. Certon, F. Teston, and F. Patat, "A finite difference model for cMUT devices," *IEEE Trans. on Ultrason., Ferroelec. and Freq. Cont.*, vol. 52, no. 12, pp. 2199–2210, Dec. 2005.

[8] G. Yaralioglu, S. Ergun, and B. Khuri-Yakub, "Finite-element analysis of capacitive micromachined ultrasonic transducers," *IEEE Trans. on Ultrason., Ferroelec. and Freq. Cont.*, vol. 52, no. 12, pp. 2185–2198, Dec. 2005.

[9] I. O. Wygant, M. Kupnik, and B. T. Khuri-Yakub, "Analytically calculating membrane displacement and the equivalent circuit model of a circular CMUT cell," in *IEEE Ultrason. Symp.*, Nov. 2008, pp. 2111–2114.

[10] S. Olcum, M. Senlik, and A. Atalar, "Optimization of the gain-bandwidth product of capacitive micromachined ultrasonic transducers," *IEEE Trans. on Ultrason., Ferroelec. and Freq. Cont.*, vol. 52, no. 12, pp. 2211–2219, Dec. 2005.

[11] M. Kupnik, I. O. Wygant, and B. T. Khuri-Yakub, "Finite element analysis of stress stiffening effects in CMUTs," in *IEEE Ultrason. Symp.*, Nov. 2008, pp. 487–490.

[12] S. Wong, R. Watkins, M. Kupnik, K. Pauly, and B. Khuri-Yakub, "Feasibility of mr-temperature mapping of ultrasonic heating from a CMUT," *IEEE Trans. on Ultrason., Ferroelec. and Freq. Cont.*, vol. 55, no. 4, pp. 811–818, April 2008.

[13] B. Bayram, G. Yaralioglu, M. Kupnik, A. Ergun, O. Oralkan, A. Nikoozadeh, and B. Khuri-Yakub, "Dynamic analysis of capacitive micromachined ultrasonic transducers," *IEEE Trans. on Ultrason., Ferroelec. and Freq. Cont.*, vol. 52, no. 12, pp. 2270–2275, Dec. 2005.

[14] J. Chen, X. Cheng, C.-C. Chen, P.-C. Li, J.-H. Liu, and Y.-T. Cheng, "A capacitive micromachined ultrasonic transducer array for minimally invasive

medical diagnosis," *J. Microelectromech. Syst.*, vol. 17, no. 3, pp. 599–610, June 2008.

[15] I. Wygant, M. Kupnik, J. Windsor, W. Wright, M. Wochner, G. Yaralioglu, M. Hamilton, and B. Khuri-Yakub, "50 khz capacitive micromachined ultrasonic transducers for generation of highly directional sound with parametric arrays," *IEEE Trans. on Ultrason., Ferroelec. and Freq. Cont.*, vol. 56, no. 1, pp. 193–203, January 2009.

[16] I. O. Wygant, M. Kupnik, B. T. Khuri-Yakub, M. S. Wochner, W. M. Wright, and M. F. Hamilton, "The design and characterization of capacitive micromachined ultrasonic transducers (CMUTs) for generating high-intensity ultrasound for transmission of directional audio," in *IEEE Ultrasonics Symp.*, Nov. 2008, pp. 2100–2102.

[17] M. Averkiou, "Tissue harmonic imaging," in *Ultrasonics Symposium, 2000 IEEE*, vol. 2, Oct 2000, pp. 1563–1572 vol.2.

[18] M. Greenspan, "Piston radiator: Some extensions of the theory," *Acoustical Society of America Journal*, vol. 65, pp. 608–621, Mar. 1979.

[19] G. Yaralioglu, M. Badi, A. Ergun, and B. Khuri-Yakub, "Improved equivalent circuit and finite element method modeling of capacitive micromachined ultrasonic transducers," in *IEEE Ultrasonics Symp.*, vol. 1, Oct. 2003, pp. 469–472 Vol.1.

[20] A. Bozkurt and M. Karaman, "A lumped circuit model for the radiation impedance of a 2D CMUT array element," in *IEEE Ultrasonics Symp.*, vol. 4, Sept. 2005, pp. 1929–1932.

[21] S. A. Maas, *Nonlinear microwave and RF circuits. 2nd ed.* Artech House, 2003.

[22] J. Liu, D. Martin, T. Nishida, L. Cattafesta, M. Sheplak, and B. Mann, "Harmonic balance nonlinear identification of a capacitive dual-backplate

MEMS microphone," *J. of Microelectromech. Sys.*, vol. 17, no. 3, pp. 698–708, June 2008.